

MICROTHERMOMETRY AND RAMAN SPECTROSCOPY OF FLUID AND MELT INCLUSIONS IN THE ALPINE PORPHYRY COPPER DEPOSITS FROM ROMANIA: INSIGHTS ON MICROMETALLOGENY

Ioan PINTEA^{1*}, Sorin Silviu UDUBAȘA², Elena Luisa IATAN³, Ion BERBELEAC³, Daniel BÎRGĂOANU¹, Oana Claudia CIOBOTEA-BARBU¹, Eduard GHINESCU¹

¹Geological Institute of Romania, 1, Caransebeș Str., 012271 Bucharest, Romania;

²Univ. of Bucharest, 1, N. Bălcescu Blv., 010041 Bucharest, Romania;

³Institute of Geodynamics of Romanian Academy, 19-21, J.-L. Calderon Str., 020032 Bucharest, Romania.

* ipinteafincs@yahoo.com

Abstract: The paper presents complementary analyses of Raman spectroscopy and high-temperature microthermometry on fluid/melt inclusions from alpine porphyry copper and associated epithermal and skarn deposits from Romania. It reveals a complex phase association and multistage evolution during the magmatic-to-hydrothermal processes underlying the deep-seated MASH zones of the related subduction factories. Important differences in P-T-X properties were found for the main mineralizing processes between the two porphyry copper deposit clusters, one in the Banat region of the South Carpathians (Upper Cretaceous) and other in the Metaliferi Mountains of the South Apuseni Mountains (Miocene). These differences ranged up to 300°C in temperature, more than 1-3 kbar of pressure and 20-30 wt% NaCl eq. salinity. Although the magmatic-hydrothermal transitions are characterized by melt-melt-fluid immiscibility at high P-T conditions in both regions.

Detailed complementary microthermometry and Raman spectroscopy show regularity during heating/quenching cycles indicating successive phase transitions of multiple daughter minerals in hydrosaline melt inclusions. Complex hydrous saline phases, including javorieite-like, halite, anhydrite, magnetite, hematite and sulfide as triangular chalcopyrite (identified before and after microthermometry by Raman spectroscopy) behaved as true daughter minerals precipitated from the hydrosilicate liquid inside the trapped singular or coeval silicate-hydrosaline melt inclusions starting from about 1085°C, the estimated trapping temperature by microthermometry. The same successive phase transitions are envisaged to proceed during the formation of the alteration-mineralization assemblages characteristic to typical porphyry copper genesis.

Keywords: hydrosaline melt inclusions, microthermometry, Raman spectroscopy, porphyry copper deposits, Carpathians, Romania

1. Introduction

Fluid-melt evolution and ore elements transport and deposition during the formation of porphyry copper systems is a complex process involving fluid phase separation from various magma compositions and batches situated at different depths above the subduction zones from Upper Cretaceous and Miocene environments in the Carpathian regions from Romania. These processes took place over large P-T-X conditions from orthomagmatic to multiple hydrothermal episodes starting above 1000°C and frequently finished under 100°C, from more than 2kb to less than 100bar, and salinity from less than 10 wt% NaCl eq. to more than 80 wt% NaCl eq. (Pintea, 2014 and references therein). Magmatic immiscibility between hydrosilicate melt, hydrosaline melt, sulfate ± carbonate ± phosphate ± chloride ± fluoride vapor-rich “melt”, sulfide and oxide melt took place during first and secondary boiling in potassic and phyllic assemblages, followed by successive boiling episodes which deposited ore minerals in the argillic and propylitic alteration zones. The ore elements are redistributed amongst various solid phases, which generally could be identified as daughter mineral phases in silicate, hydrosaline and aqueous inclusions from ubiquitous quartz in characteristic veinlets in the stockworks structures of the porphyry copper systems. This study uses microthermometry and Raman spectroscopy to provide useful insights on micrometallogeny from the behavior of the included phases after trapping suggesting that similar characteristics generally apply to porphyry Cu-(Au)-(Mo) formation.

1.1. Materials and methods

Doubly polished quartz thin sections and wafers were used for petrography, microthermometry and Raman spectroscopy. Microthermometry of silicate melt-hydrosaline melt inclusions were measured in a “home-made” heating stage up to 1100°C under the microscope. The heating stage was calibrated with K₂Cr₂O₇ (398°C), α-β quartz transition temperature (573°C), NaCl (801°C), gold (1064°C). A kanthal heating element was used for heating, and maximum quenching was simply done by cutting off the electrical power. The heating rate ranged from 5° to 100°/min in variable combination steps and quenching rate by 50° to 200°/min. The duration of a complete heating-cooling cycle in hydrosaline melt

inclusions ranged between 10 min to more than 1.5 hours. The relative accuracy of phase change measurements ranged between 86-99.5%. Calculated P-T-X data were based upon the SoWat software (Driesner and Heinrich, 2007; Driesner, 2007). It is worth noting that when entrapment of the fluid phases is heterogeneous, i.e. two or more fluid phases were trapped together in the same cavity, the recorded P-V-T-X-properties are not representative of the initial formation conditions of the complex silicate-hydrosaline melt inclusions but the microthermometry could be used to characterize the nature of included phases and their physical (immiscibility) chemical (ore element partitioning) inter-relationships.

Vibrational Raman spectra of solid daughter phases (transparent and opaque) from both porphyry copper provinces were performed at the Geological Institute of Romania on a Raman Renishaw spectrometer equipped with a Leica DM 2700M microscope and 50x objective lenses. Excitation was provided by two laser types with 532 nm with grating of 1200 grooves/mm and 1800 grooves/mm and 785 nm with grating of 1200 grooves/mm, respectively. The spectral resolution was +/- (1-2) cm^{-1} and laser exposure ranged between 5 to 15 sec with spectral accumulations from 1 to 55.

Decrepitated mound analysis is a complementary method used to estimate the chemical and mineralogical composition of thermally decrepitated fluid inclusion and successfully used, especially in exploration targets. There are several papers published in the literature which deal with sample analysis procedure starting with sample collection in the field, fluid inclusion selection for decrepitation study, analytical protocols on SEM-EDS and electron microprobe (Haynes et al., 1988; Heinrich and Cousens, 1989; Kontak, 2004; Kontak, 2013; Tweedale et al., 2015). The decrepitated mounds of the brine inclusions formed accidentally during microthermometry in the same assemblages such as those used in recorded phase transition were also analyzed tentatively by Raman spectroscopy. To prevent atmospheric hydration, the used quartz section fragments were immediately sealed in aluminum foil. During analysis, the laser was focused on several points of the concentrically deposited mound including the former cavity bottom.

2. Geological setting

There are two main regions of porphyry copper and related epithermal and skarn deposits occurrences in Romania:

1. The Late Cretaceous Banatitic (Laramide) province in the Banat region which belongs to the 1500 km - long of Apuseni – Banat – Timok – Srednogorie magmatic-metallogenetic belt in the Carpathian-Balkan orogen formed on the European margin during the closure of the Neotethys Ocean (Ciobanu et al., 2002; Zimmerman et al., 2008; Ilinca et al., 2011; Gallhofer, 2015). The magmatic arc was active for ~25 Myr (~92-67 Myr – Gallhofer, 2015).

2. The Miocene porphyry copper cluster from the “Golden Quadrangle” in the Metaliferi Mountains, which includes around 20 porphyry-epithermal Cu-Au(Mo) and related magmatic-hydrothermal deposits/prospects of the Hălmagiu - Brad - Săcărâmb, Zlatna - Stănița, Bucium - Roșia Montană - Baia de Arieș volcano-tectonic basins, with extension in Zarand (Tălagiu) and Poiana Ruscă Mountains (Deva) (Udubașa et al., 2001; Roșu et al., 2004; Berbelec et al., 2014).

Additionally, possible prospective areas include the Eastern Carpathian from Baia Mare mining district (e.g. Nistru; Oaș, SE-Gutâi Mountains and Țibleș massif,) and Călimani-Gurghiu-Harghita volcanic chain (e.g. tourmaline indicative mineral in the South Harghita region) – Pinteș et al. (1999), Damian (2003), Pinteș and Laczko (2005), Vlad (2011), Pinteș (2016).

The porphyry copper deposits consist of small-sized, intrusive stocks with concentric alteration zones which exhibit similarities with the Lowell and Guilbert (1970) model during Laramian times and with the Hollister (1975) diorite model during Miocene times.

The spatial distribution of the porphyry ore bodies seems to be controlled by N-S Laramian tectono-magmatic alignments (Banat) and NW trending Neogene basins controlled by crustal faults (Metaliferi Mountains). The Laramian porphyry Cu mineralizations are intimately associated with intrusive bodies and skarn deposits and Neogene ores with volcanic structures (Ianovici et al., 1977).

2.1. Upper Cretaceous porphyry Cu-Mo (Au) deposits in the Banat Mountains metallogenetic sub-belt

The Romanian sector of the Late Cretaceous Banatitic Magmatic and Metallogenetic belt contains plutons (granitoids), volcano-plutonic complexes and related dikes (calc-alkaline, I-type granitoids), with related ores and shoshonitic plutons that lack economic interest (Fig. 1). Cu (Mo) ores in skarn/porphyry deposits are related to plutonic apophyses along a major N-S Oravița-Ciclova-Sasca-Moldova Nouă alignment of the South Banat Mts (Vlad and Berza, 2003). Mineral deposits within the

Cretaceous Banatitic Magmatic and Metallogenic belt are strongly differentiated with respect to the host rock types and depth of magma emplacement. Copper and base metal skarn deposits form the most widespread metal accumulations. Porphyry copper ores with Cu ± Au, Ag, Mo are hosted by shallower hypabyssal bodies: e.g., Moldova Nouă. Subeconomic porphyry copper (± Mo) accumulations are also present at Oravița, but the hydrothermal alteration is far less pervasive than at Moldova Nouă. Large shallow porphyry-style systems with pyrite halos (and/or skarn halos) extend only south of Poiana Ruscă but they lack economic mineralization. Some occurrences are set apart by prominent Fe metallogeny (e.g., Ocna de Fier, Mașca Băișoara) (Ilinca, 2012).

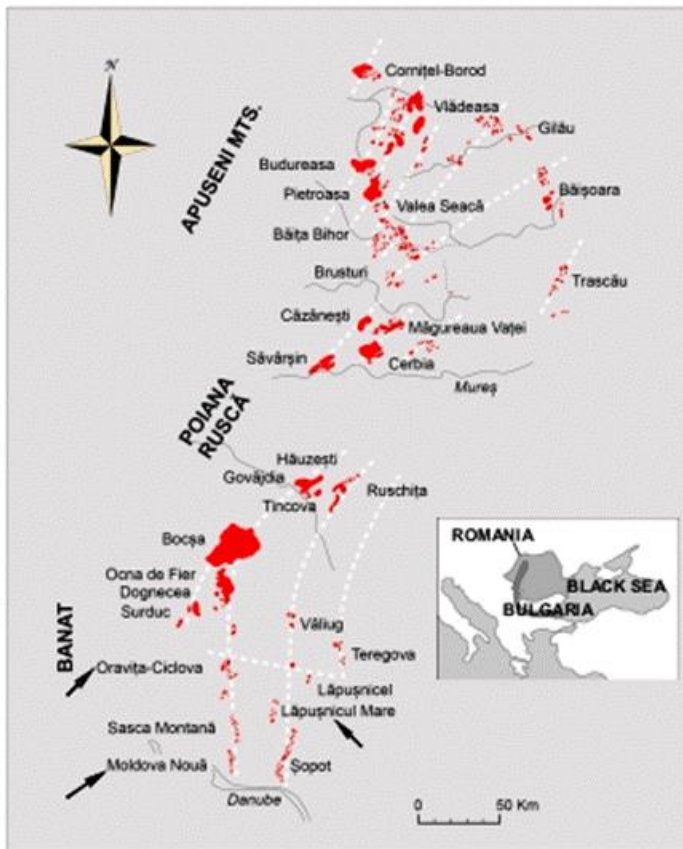


Fig.1. The banatitic belt from Romania with petrogenetic alignments and banatitic massif containing the porphyry Cu-Au-Mo deposit in the Banat region (arrows) – modified from Ilinca et al. (2011).

2.2. Miocene porphyry Cu-Au (Mo) deposits in the Apuseni Mountains

The porphyry copper deposits from the Apuseni Mountains are associated with the Miocene magmatism and metallogenic activity (Fig. 2). Magmatic-volcanic products' geochemistry reflects a gradual evolution, from normal (14.8-11 Myr) and "adakitic-like" calc-alkaline products (12.6-7.4 Myr), to the latest magmatic products having alkaline features (Roșu et al., 2004).

Porphyry-epithermal hydrothermal systems are centered on the volcanic structures, being genetically related to porphyritic, andesite-microdiorite subvolcanic bodies. The porphyry copper deposits from Apuseni Mountains can be divided into three types: Cu-Mo (Au) type (Deva, Rosia Poieni), Cu-Au type (Valea Morii, Bolcana, Rovina, Voia, Talagiu, Larga, Trâmpoiele, Valea Tisei, Tarnita) and Au-Cu porphyry type (Colnic, Ciresata) (Cioacă and Munteanu 2012).

3. Mineralization- alteration characteristics

3.1. Upper Cretaceous

Skarn mineralizations occur commonly as lenses and irregular bodies with branching apophyses in the vicinity of igneous apices and display no striking mineral zoning. The Cu ores consist commonly of chalcopyrite + pyrite + molybdenite (Bozovici), pyrite + chalcopyrite + molybdenite + magnetite + tetrahedrite (Moldova Nouă), pyrite + chalcopyrite + molybdenite + scheelite + gold (Oravița), pyrite + chalcopyrite + scheelite (Ciclova), (Table 1). Dissemination is dominant in the potassic zone while fracture filling is the most important in the phyllic zone (Ianovici et al., 1977).

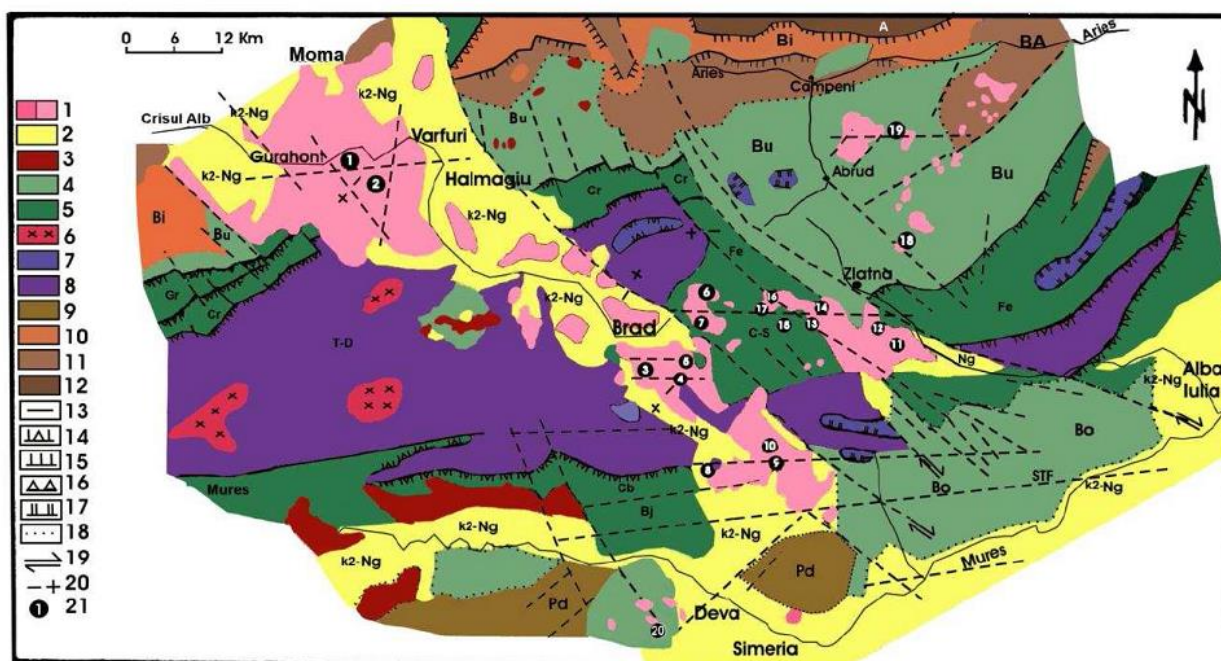


Fig. 2. Sketch map of the South Apuseni Mountains with the location of porphyry epithermal Cu - Au (Mo) and epigenetic hydrothermal deposits/prospects (simplified after the Geological Map of Romania edited by Geological Institute of Romania, scale 1: 50,000, Abrud, Zlatna, Geoagiu, Deva, Brad, sheets; modified by Berbeleac et al., 2005). 1. Tertiary volcanic rocks: a. Neogene and b. undifferentiated volcanics (Uroi trahyandesite rocks); 2. K₂-Ng: Fața Băii Fm. - Upper Cretaceous-Neogene sedimentary deposits; 3. K₂-Pg: Banatitic rocks undifferentiated; Late Cretaceous Fm. (dominantly Bucium Unit); 5. Early Cretaceous Fm. (dominantly Feneș nappe); 6. Jurassic granitoides; 7. Ardeu nappe and others; 8. Jurassic ophiolite (Drocea-Techereu nappe); 9. Padeș crystalline schists (Pz); 10. Biharia nappe system - shear zone; 11. Baia de Arieș series (Pcb); 12. Feniș-Gîrda nappe; 13. geological boundary; 14. K₂-Pg nappes; 15. Pre-Gossau nappes; 16. Variscan nappes; 17. Mesocretaceous nappes; 18. Unconformity; 19. Thrust faults; 20. Normal fault and block movement; 21. Ore deposits/prospects. A- Feniș Gîrda nappe, Bo- Bozeș nappe, Bu- Bucium nappe, Bi- Biharia nappe, Ba- Baia de Arieș nappe, Bj- Bejani nappe, Cb- Căbesti nappe, T-D- Techereu-Drocea, Cr- Criș, Gr- Groși, C-S- Curechiu-Stănița, STF- South Transylvania Fault. Ore deposits/prospects: 1. Tălagiu North, 2. Tălagiu Central South, 3. Musariu, 4. Valea Morii Nouă, 5. Cireșata, 6. Remetea, 7. Colnic, 8. Bolcana, 9. Voia, 10. Voia North, 11. Fața-Băii - Larga, 12. Trâmpoiele, 13. Muncăceasca Vest, 14. Popa-Stănița, 15. Măgura Poieni, 16. Valea Tisei, 17. Runculeț, 18. Bucium Târnița, 19. Roșia Poieni, 20. Deva. Modified from Berbeleac et al. (2014). Metaliferi Mountains: Lat. 46°18'(46.3°) N and Long. 22°50'(22.8333°) E, from <http://map.carta.com/>.

Table 1. Main geologic features of the Upper Cretaceous porphyry Cu-(Mo)-Au deposits from Banat region (Southwestern Romania).

Deposit, Elements	Mineralization type, Host Rock	Alteration	Ore mineralogy	Ore deposit morphology
Lapusnicu Mare Cu	skarn, quartz monzodiorite	propylitic, argillic	cpy, py, po, mo, hem, mgt, sph	impregnations
Moldova Noua Cu	skarn, porphyritic granodiorite, monzodiorite, diorite, carbonate sedimentary (J-K age)	potassic, phillic, propylitic	mgt, ccp, py, sph, mo, ttr, bn, gn	impregnations, disseminations, veinlets
Ciclova Montana Cu-Mo (W)	skarn, granodiorite, carbonate sedimentary (J age)	phillic, argillic, propylitic	py, ccp, gn, sph, mo, mgt, hem, ttr, bis, schl	stockworks, lenses, impregnations
Oravita Cu (Mo, W, Bi)	skarn, granodiorite, diorite, gabbro, paleozoic pelites, carbonate sedimentary (J-K age)	phillic, argillic, propylitic	ccp, py, mgt, hem, bn, mo, po, sph, ttr, schl	stockworks, lenses, impregnations

Mineral abbreviations: cpy - chalcopyrite, py - pyrite, po - pyrrotite, mo - molybdenite, hem - hematite, mgt - magnetite, sph - sphalerite, ttr - tetrahedrite, bn - bornite, gn - galena, bis - bismuthinite, schl - scheelite.

In relation to the degree of alteration, porphyry copper deposits show a spatial zonation of ore minerals. In the central parts of the mineralized body, the phyllic alteration is dominant (sericite-quartz ± chlorite) where magnetite, hematite, pyrite, chalcopyrite, ± bornite, ± molybdenite and secondary Cu minerals are present (Fig. 3). Peripheral, the propylitic alteration is associated with other alteration types such as the argillic zone, with variations in the upper part of the structure (quartz, argillic minerals,

alunite, anhydrite, chlorite, albite) where pyrite, marcasite, \pm sulfides are present. The main by-products of this type of ores are: Mo, Au, Fe, Ti, Pb, Zn, Cd, In, etc. (Cioacă and Munteanu, 2012).

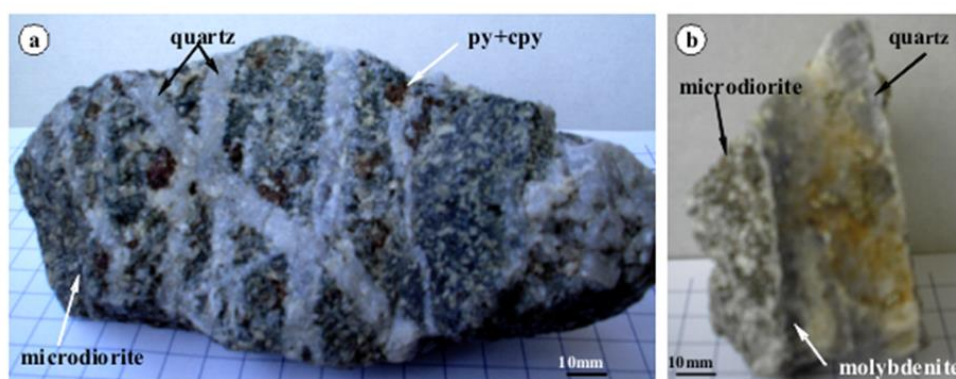


Fig. 3. Characteristic quartz veinlets in the porphyry Upper Cretaceous Cu-Au-Mo deposits from **a.** Lăpușnicu Mare and **b.** Moldova Nouă in the Banat region (South Carpathians); py - pyrite, cpy - chalcopyrite.

3.2. Miocene

Miocene porphyry copper deposits of the Apuseni Mountains show affinities towards the dioritic model. They contain pervasive potassic alteration with disseminated grains, veins and veinlets of pyrite + chalcopyrite (Tarnița, Rovina, Valea Morii, Bolcana), pyrite + chalcopyrite + molybdenite (Roșia Poieni) and quartz + bornite + chalcopyrite \pm calcite \pm fluorite (Deva), (Table 2), surrounded by the argillic zone (Fig.4). In some places, a larger scale zonality is provided by the axial setting of porphyry copper-bearing subvolcanoes surrounded and even cut by base metal veins connected with adjacent volcanic structures (e.g. Valea Morii - Ianovici et al., 1977; Kouzmanov et al., 2010).

Porphyry copper ores of the Apuseni Mountains show an evolution from acid to neutral regimes, highlighted by the mineral association with Fe oxides.

Table 2. The main characteristics of the Miocene porphyry Cu-Au-Mo deposit from the Metaliferi Mountains (South Apuseni Mountains, Western Romania).

Deposit Elements	Host Rock	Alteration	Ore mineralogy	Ore deposit morphology
Rosia Poieni Cu-Au (\pm Mo)	qtz andesite, amph-andesite, microdiorite	potassic, phyllic, propylitic, advanced argillic	py, cpy, bn, mgt, mo, hem, ttr, tenn, po, sph, gn, en, Au, Ag, cc, cv, anh, alu, dg, tld, ru, viv	impregnations, disseminations breccias, veins, veinlets
Tarnita Cu-Au (\pm Mo)	amph-andesite, microdiorite	potassic, phyllic, propylitic, argillic	py, cpy, mgt, bn, mo, hem, ttr, po, sph, gn, Au, cc, cv, anh, alu, dg, ru, viv	impregnations, veins, breccias
Bolcana Cu-Au (\pm Mo)	microdiorite, amph-andesite	potassic, phyllic, propylitic, argillic	cpy, py, mgt, hem, bn, Au, cv, cc, ttr, sph, gn, po, mo, ru, alu, anh	impregnations, veins, breccias
Valea Morii Cu-Au (\pm Mo)	andesite, qtz-diorite, amph-px microdiorite	potassic, phyllic, propylitic, argillic	cpy, py, mt, mo, bn, sph, gn, Au, ru, alu, anh	stockwork, veinlets, veins
Deva Cu-Au (\pm Mo)	andesite, microdiorite, granodiorite	potassic, phyllic, propylitic, argillic	bn, cpy, mgt, py, cv, hem, Au, mo	impregnations, veins, breccias
Talagiu Cu-Au (\pm Mo)	andesite, microdiorite	potassic, phyllic, propylitic, argillic	py, cpy, bn, mgt, hem, Au, Ag, sph, tld, alu, anh, ru, gy	impregnations, veins, breccias

Mineral abbreviations: py – pyrite, cpy - chalcopyrite, bn – bornite, mgt – magnetite, mo – molybdenite, hem – hematite, ttr – tetrahedrite, tenn – tennantite, po – pyrrhotite, sph – sphalerite, gn – galena, en – enargite, Au – native gold, Ag – native silver, cc – chalcocite, cv – covellite, anh – anhydrite, alu – alunite, dg – digenite, tld – tellurides, ru – rutile, viv – vivianite, gy – gypsum.

4. Fluid and melt inclusion study

In this paper, we intend to complement the extended review paper published by the first author (Pintea, 2014) with some new microthermometric experiments on silicate melt-hydrosaline melt inclusions in quartz from both porphyry Cu-(Au)-(Mo) districts from Romania by adding specific information about the microthermometric behavior of halite, anhydrite, magnetite/hematite and

chalcopyrite daughter minerals from specific brine inclusion assemblages. Many of these microthermometric measurements were preceded and/or postdated by Raman microspectroscopy for solid species identification in the same or similar inclusions. In the next step of this study, we intended to record the individual Raman spectra for each above-mentioned phase during heating and quenching. This is based upon the idea that the named phases are true daughter minerals precipitated from a complex hydrosilicate–hydrosaline mixture forming primary isolated or consistent microfissure healing assemblages. Moreover, it is presumed that the majority of ore elements are partitioned amongst silicate and hydrosaline phases following a fractionation descent line starting from orthomagmatic stages and finishing at epithermal ones.

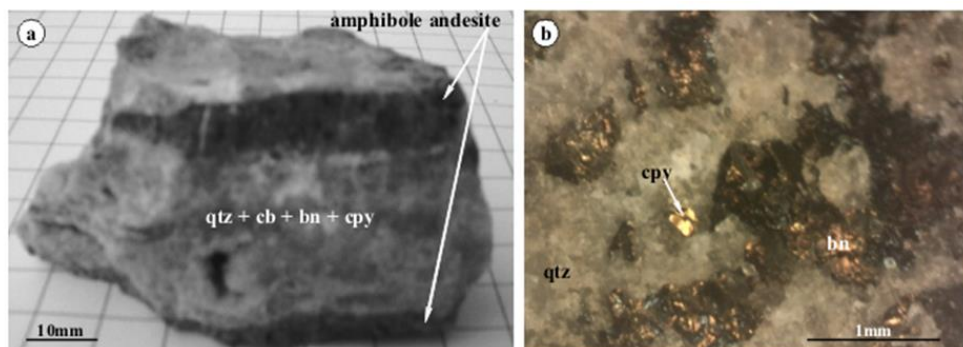


Fig. 4. Quartz-carbonate-bornite-chalcopyrite veinlet from Deva porphyry Cu-Au-Mo deposit (Miocene), **a.** transversal section, and **b.** longitudinal section; qtz - quartz, cb – calcite, cpy - chalcopyrite, bn - bornite.

4.1.1. Silicate melt - hydrosaline melt immiscibility in porphyry copper systems

Heterogeneous silicate-hydrosaline-sulfide/oxide assemblage was first described in Romania at the Miocene Deva porphyry Cu-Au (Mo) by Pintea (1993) followed by the evidence that this is a common process during magmatic-hydrothermal transition in all the porphyry deposits and occurrences from the Miocene in the Metaliferi Mountains and Eastern Carpathians, and also in the Upper Cretaceous in the Southern Carpathians, especially at Moldova Nouă and Oravița mining prospects from the Banat region in Romania. Preliminary data on the microthermometry of glass and hydrosaline melt inclusions from these deposits were presented in an unpublished Romanian Geological Institute report (Pintea in Roșu et al., 2002) and a published extended abstract (Pintea, 2002; Fig.5). It was evident that there are important differences regarding the content and microthermometric behavior of silicate-hydrosaline phases from the two mentioned regions during the main stages of mineralization, i.e. Miocene vs. Upper Cretaceous. Firstly, homogenization temperatures and halite dissolution temperatures in the Upper Cretaceous are up to 150°-300°C less than in the Miocene porphyry deposits, and also the salinity shows differences of about 20-30 wt% NaCl eq. Secondly, the homogenization temperatures in complex silicate-hydrosaline inclusions show lower values of around 300°C and less than 1-3 kb pressure in the Upper Cretaceous samples. One possible explanation of these differences was emphasized for the Miocene prospects from the Metaliferi Mountains (Pintea, 2014) with respect to the tectonomagmatic events related to the orientation of the subduction plane and asthenospheric thermal regime in the mantle wedge. More information based upon geodynamic models and magmatic-hydrothermal controls on porphyry systems especially Cu(-Mo-Au) deposits in the last decades can be found in some recently published papers (e.g. Udubașa et al., 2001; Richards, 2009; Harris et al., 2013; Gallhofer, 2015; Audétat and Simon, 2012; Kouzmanov and Pokrovski, 2012, and references therein).

During the heating procedure under the microscope stage, the complex, nearly crystalline silicate glass-hydrosaline melt, together with the opaque phase, become an emulsion containing two globules of salt melt floating in the hydrosilicate liquid phase at high temperature (Fig.6). The two opaque particles, one triangular and another globular (at room temperature) still remain undissolved at the bubble homogenization temperature (892°C) and both of them seem to be in the liquid state at this temperature. On further heating one of them (probably hematite) melted completely at 912°C (20°C after the bubble homogenization temperature). The remaining opaque liquid globule is still there at 988°C (Fig.6-j), and is probably a liquid sulfide. In other similar inclusion the opaque liquid globule remained up to 1037°C, and probably turned into copper chloride at such high temperature (e.g. Hack and Mavrogenes, 2006). On quenching, the vapor bubble appeared first suddenly, perhaps with an attached solid oxidic phase.

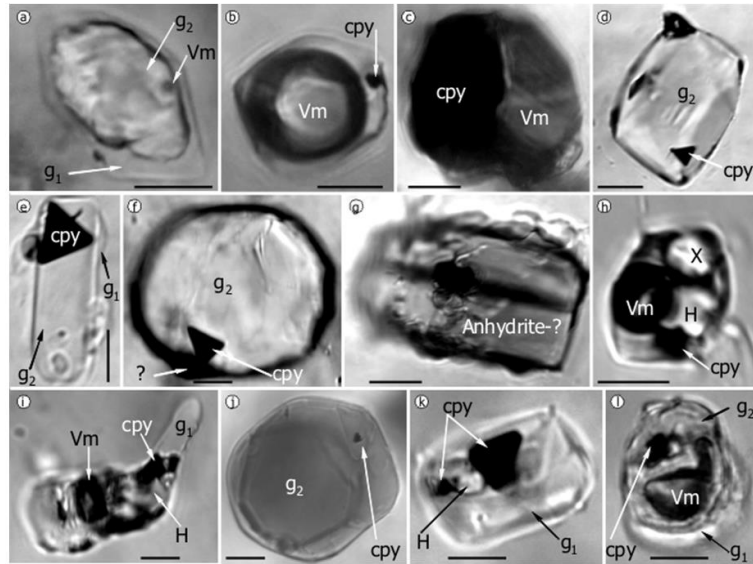


Fig. 5. Fluid and melt inclusions types in Upper Cretaceous porphyry copper deposits from the Banat metallogenetic sub-belt. Notations: g1, g2- glass; Vm- vapor-”melt”, cpy- chalcopyrite, H- halite, X – unidentified crystal; Scale bar: 10µm.

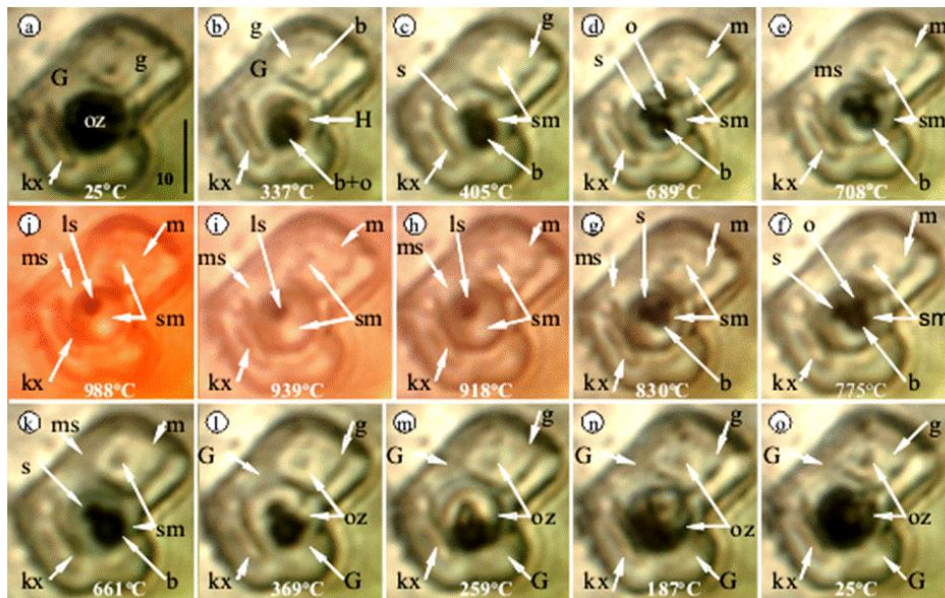


Fig. 6. Silicate melt - salt melt microthermometry showing immiscibility in a glassy inclusion from coarse grain quartz from Oravița porphyry Cu-Mo-(Au) prospect (Nicolae adit). Notations: G- glass, g- another glass, kx- anhydrite, H- halite, b- bubble, o- opaque, sm- salt melt, m- another melt, ms- silicate melt, s- sulfide (chalcopyrite), ls- liquid sulfide, oz- ore fluid (bubble+halite+opaque+other phases). Scale bar: 10µm.

Then the sulfide liquid solidified and turned into a triangular shape (probably chalcopyrite) and also remained in contact with the bubble assemblage. The main two salt globules remain rounded but are developed around some elongated grains inside the hydrosilicate liquid above 600°C. These elongated phases are perhaps sulfate or carbonate phases and do not melt completely during heating. On further quenching, the halite renucleated more evidently in the bigger salt globule. The hydrosilicate liquid solidified as amorphous silicate glass, around 500°C, or less. Calculated values by SoWat program for halite dissolution temperature $T_{mH}=401^{\circ}\text{C}$ and $T_{\text{bubble}}=892^{\circ}\text{C}$ give a pressure of $P=1784.59$ bar, salinity $W_s=47.2345$ wt% NaCl eq., density $d=0.831571$ g/ccm, with molar NaCl fraction $x=0.21$, and originally trapped fluid was in the V+L phase state.

The hydrosilicate melt phase in these inclusions has shown an uncommon complex composition suggesting the presence of a “clathrasil” compound (hydrosilicate of K,Na, Ca, etc), or a “zeolitic” melt framework (e.g. Momma, 2014). Generally, the silicate glass phase seems to contain carbonate, sulfate and phosphate radicals as the Raman spectra suggested (Fig. 7).

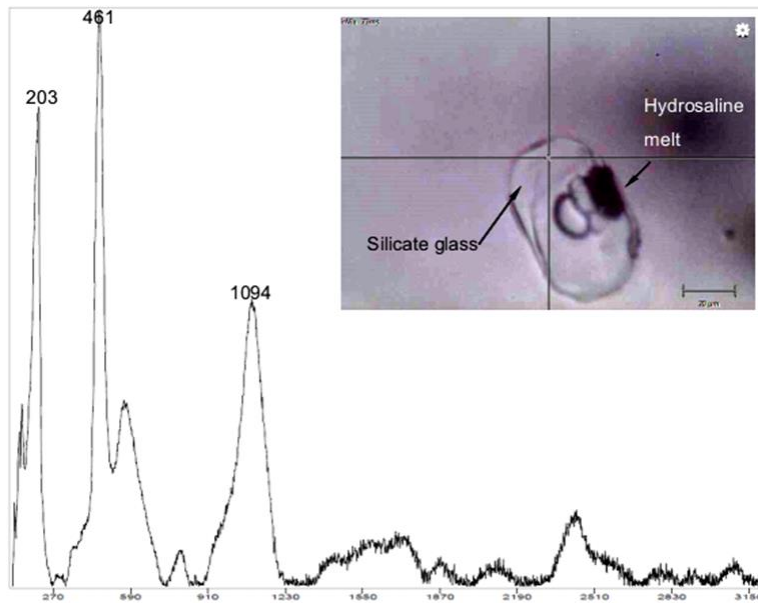


Fig. 7. Raman spectra of silicate glass component in complex silicate-hydrosaline melt inclusion in quartz from Oravița porphyry Cu-Mo-Au prospect (Upper Cretaceous, Banat region). This is indicative of the presence of CO_3^{2-} stretching line at 1094 cm^{-1} ; 203 and 461 cm^{-1} being the significant peaks of hosting quartz (Frezzotti et al., 2012). Scale bar: $20 \mu\text{m}$.

Ultimately, minuscule salt daughter phases solidified too under quenching (they melted first during the heating cycle), probably zeolites (see Stefanova et al., 2014). This kind of microthermometric behavior suggests that all the non-silicate phases were segregated from the main hydrosilicate liquid as temperature decreased, resulting in a complex melt-melt-fluid immiscibility.

Fluid inclusion studies in the porphyry copper system from Banat region (Upper Cretaceous) were done at Moldova Nouă prospect (Gheorghiiță, 1975), Lapușnicul Mare area by Pomârleanu and Întorsureanu (1985) and by Pintea, in an unpublished IGR report (Roșu et al., 2002). It was noticed that there are many types of fluid and melt inclusions especially in the characteristic quartz veinlets (some types in Fig.5) and their P-T-X-properties ranged widely between magmatic-to-epithermal (and skarn) stages (Pintea, 2002, and unpublished report - 2002) from $\geq 980^\circ\text{C}$ - 1100°C , 1-1.5 kb, 60-87 wt% NaCl eq. and 4-5 wt% H_2O where silicate melt, hydrosaline melt, volatile species and around 30 vol% of crystallized phases are present; the porphyry copper formation started during the magmatic to hydrothermal transition at $\leq 980^\circ\text{C}$ - 450°C , 0.3-1.0 kb and 40-70 wt% NaCl eq. to ≤ 35 -40 wt% NaCl eq. and 450°C - 200°C and $<1.0 \text{ kb}$, which is the main stage of mineralization formation (Fig. 8); the final stages were characterized by low salinity fluids ($<5 \text{ wt\% NaCl eq.}$) where aqueous liquid solution and low-density vapor phase are coexistent.

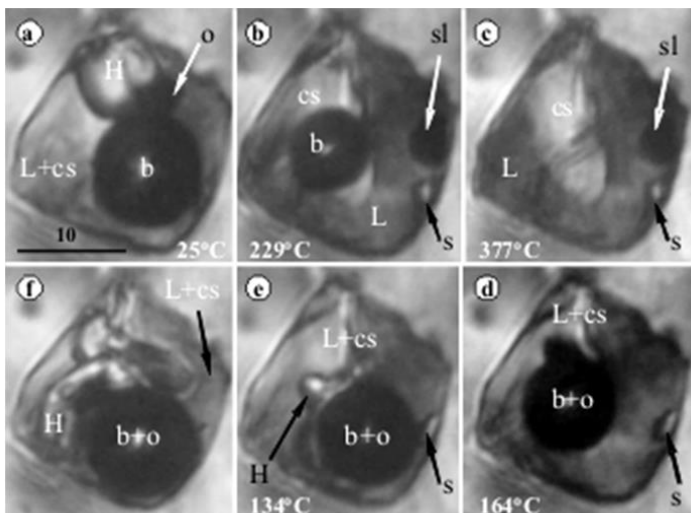


Fig. 8. Typical brine inclusion microthermometry in quartz from the main stage of mineralization of the Moldova Nouă porphyry Cu-Mo-(Au). Notations: L-liquid, H- halite, cs- catharasil, b- vapor bubble, o- opaque (chalcopyrite?), sl- liquid sulfide globule, s- unknown solid, Tm- melting temperature, Th- homogenization temperature, Tn- renucleation temperature. Scale bar: $10 \mu\text{m}$.

During microthermometry, the brine inclusion type, as an example, is presented in successive microphotographs in Fig. 8. The first phase melting is around 100°-150°C; the halite melted around 250°-350°C and partial homogenization by bubble disappearance rarely exceeded 400°-450°C for the main stage of mineralization. The opaque phase is presumed to be chalcopyrite and becomes rounded at about halite melting temperature but still remains as an opaque liquid globule after vapor bubble homogenization temperature. On quenching, the vapor bubble renucleated first with some opaque phase (oxide) attached to it. Shortly after, the opaque sulfide starts to form as a triangular opaque but still remained attached to the vapor bubble. An unknown white solid phase (perhaps a clathrasil compound, precipitated immediately after sealing, but never remelted) remains unchanged in shape and volume. Halite renucleated as several particles, which immediately start to coagulate by Ostwald ripening. After several microthermometric cycles, the composition does not seem to be changed and all phases melted and renucleated in the same order. SoWat calculated values, for $T_{mH}=298^{\circ}\text{C}$ and $T_{hbubble}=363^{\circ}\text{C}$, are: pressure, $P=136.265$ bar, salinity, $W_s=37.5702$ wt% NaCl eq., density, $d=1.02705$ g/ccm, with NaCl molar fraction $x=0.16$, and the original trapped fluid was a single-phase state. On quenching, the bubble renucleated suddenly at 352°C , and halite at 137°C . It is worth noting that after the second microthermometric cycle in the same inclusion the homogenization temperature slightly increased, so it is better to avoid multiple cycling, but even so the renucleation of the melted phases still remains in the same reversed order.

4.1.2. Immiscibility in the Miocene deposits from the Metaliferi Mountains

The best example of multiple immiscibility at high temperature and various pressure conditions is represented by the complex silicate glass-hydrosaline melt inclusions from Deva porphyry Cu-Au-(Mo) prospect in the Metaliferi Mountains from the South Apuseni region in western Romania (Fig. 2). Moreover, they are also coexistent with a sulfide-rich phase represented especially by bornite and chalcopyrite (Pintea, 1993; 1995; 1996a, b; 2014; Fig. 4). In these veinlets, multiple melt inclusion types which delineate specific assemblages as primary random silicate melt, salt melt, hydrosaline melt and vapor-rich inclusions, some of them showing very high and uncommon homogenization temperatures, up to around 1400°C , were described (Pintea, 2014, and reference therein). Recently similar observations were reported at Grasberg porphyry Cu-Au from the Late Pliocene Ertsberg-Grasberg porphyry-skarn Cu-Au-(Mo) district in the Papua province in eastern Indonesia (Mernagh and Mavrogenes, 2019, and references therein).

During more than 25 years of investigations, various forms of immiscibility have been found in each of the Miocene porphyry copper systems from the Metaliferi Mountains (Pintea, 2014). One simple example is presented in Fig. 9 where ore fluids (vapor, salt and an opaque) are dispersed as globules of various sizes inside the hydrosilicate liquid phase. At the highest temperature (i.e. Fig. 9; 1049°C) a liquid phase surrounds both the vapor bubble and the opaque phase in the hydrosaline globule. When halite dissolution temperature can be recorded, the salinity ranged around 60wt% NaCl eq, calculated at the highest temperature in the stage, but these values are indicative because the final homogenization temperature was not achieved. Obviously, these inclusions cannot be homogenized even at very high temperatures (see Pintea, 2014) but the immiscibility is evident because the hydrosilicate glass is completely melted at such high temperatures, and SoWat program suggested heterogeneous entrapment of (V+L) phase at those temperatures.

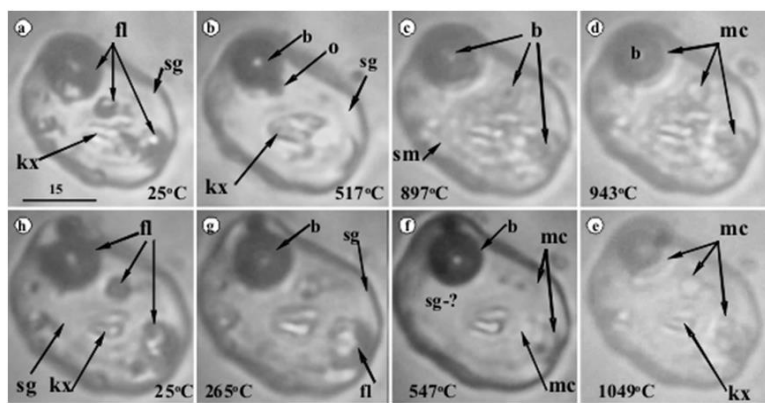


Fig. 9. Immiscibility between silicate melt and ore fluid in reheated glass inclusion in quartz from Bolcana ore deposit. Notations: of- ore fluid (bubble+halite+opaque+other phase), kx- solid, sg- silicate glass, sm- silicate melt, mc- salt melt, b- bubble, o- opaque. Scale bar: 15µm.

As it was already mentioned (Pintea, 2014) the hydrosilicate-hydrosaline-(Fe-S-O) melt immiscibility is the most prominent genesis process of porphyry copper systems from the Metaliferi Mountains and controls the entire fluid-melt evolution of the transition from magmatic-to-hydrothermal stages. The common trapping temperature in the magmatic stage (first and secondary boiling) was estimated during microthermometry by a pair of silicate melt and hydrosaline melt inclusions, based upon the beginning of silicate liquid formation in hydrosaline melt inclusion and salt melt exsolution in the contemporaneous silicate melt inclusion in the same assemblage, around 1085°C (i.e. Pintea, 1996a; 2009; 2012; 2014), which agrees with the main orthomagmatic-hydrothermal process in the Burnham model (Burnham, 1979; Bodnar, 1995; Campos et al., 2002; Drew, 2006; Becker, 2007; Bodnar, 2010). This process is perhaps completed by endogeneous auto-metasomatic gas-solid reaction (e.g. Blundy et al., 2015; Henley et al., 2017) which could be recognized based upon microtextural features (Pintea, 2010; 2014) of the quartz veinlets assemblage and cross-cutting relations (Kouzmanov et al., 2010; Silitoe, 2010). So, these are subsolidus reactions and took place especially between 550° and 850°C (60-80 wt % NaCl eq.; 1-2 kbar or more), characterizing the main porphyry ore stage formation process (potassic and phyllic alteration zones). At lower P-T-X conditions there are successive fluid events characteristic to the argillic and propylitic stages at <200°C, <23 wt % NaCl eq., and less than 100-300 bar. There are multiple mineral generations of apatite, rutile, ilmenite, quartz, anhydrite, calcite and ore minerals mainly magnetite, hematite, chalcopyrite, many of them being also formed as daughter minerals in the various melt and fluid inclusions types mentioned above. Most of these minerals can be found within a single hydrosaline inclusion suggesting that they form from a single generation of fluid flow (Mernagh, 2019, personal communication). The ore elements, especially Cu, Au and Mo, were partitioned between these melt-melt-fluid assemblages and their precipitation as economic mineralization was directly related to specific geodynamic conditions (e.g. Gallhofer, 2015).

5. Brine inclusions (hydrosaline melt) microthermometry

If all, or almost all, the solid microphases inside the hydrosaline melt inclusions or brine inclusions (see Kouzmanov and Pokrovski, 2012, for multiple term definitions), are daughter minerals then each of them should be in equilibrium with a complex hydrosilicate-saline solution (or melt) at specific P-T-X conditions until the content of the inclusions becomes homogeneous or heterogeneous function of trapping conditions. In this respect, we made a separate study of microthermometry coupled with Raman spectroscopy for the main daughter minerals such as halite, magnetite, hematite, anhydrite and triangular chalcopyrite. An interesting fact is the presence of javorieite – KFeCl_3 (Koděra et al., 2017) which seems to behave almost as a daughter phase (Kozák et al., 2017). A similar phase was noted frequently during microthermometry in several porphyry copper deposits in the Metaliferi Mountains (e.g. Pintea, 2014) and it was recorded as the first sharp melting point before halite dissolution between 256°-461°C and also tentatively indicated by a weak Raman shift at 64 cm^{-1} in the Bolcana Fe-rich porphyry Cu-Au-(Mo) deposit. The first melting points in hydrosaline melt inclusions between 88°-271°C (Pintea, 2014) are indicative for other hydrated salt complexes, sometimes the KCl daughter phase is used to estimate salinity in KCl-NaCl-H₂O system. They constantly renucleated as the last solid phases during the quenching cycle after heating by microthermometry, even around 70°C. A range of homogenization measurements have shown P-T-X data on a large scale of Th between 420° to 1300°C, 31-89 wt% NaCl eq. for salinity and 0.1 to 12.8 kbars for pressure trapping conditions (e.g. Pintea, 2012; 2014), suggesting various depth sources, fluid-phase immiscibility and/or heterogeneous trapping.

5.1. Halite microthermometry

Heterogeneous trapping involves the entrapment of several fluid and/or solid phases in one cavity, and their microthermometric behavior could be very complex and final homogenization temperature can be recorded only in the commercial high-temperature stages such as Linkam TS 1500 (Pintea, 1996). But in this case, is still possible to estimate salinity if we consider this temperature as a minimum homogenization value. As an example, in Fig. 10, the SoWat program estimated, for $T_{mH}=612^\circ\text{C}$ and $T_{h_{bubble}} \gg 1037^\circ\text{C}$, a pressure of 1312.53 bar, salinity of 75.9472 wt% NaCl eq., density of the liquid phase = 1.102 g/ccm with NaCl molar fraction $x_{\text{NaCl}}=0.5$. The original fluid was in the (V+L) phase state as it was precluded initially by visual estimation (i.e. bubble about 40-50% volume). In the same inclusion, the opaque phase melted at 786°C, another opaque melted at 1000°C, and a meniscus was formed during heating between a silicate film and the chloride-rich phase at 1000°C, suggesting immiscibility. Sulfide renucleated at 574°C (probably chalcopyrite). During heating, these complex brine inclusions (e.g. Fig. 10) homogenize at very uncommonly high temperatures (e.g. Pintea, 1996a, b; 2014;

Mernagh and Mavrogenes, 2019, and references therein), although these high-temperature values could be related to some specific geodynamic conditions as mentioned above (e.g. Pintea, 2014; Gallhofer, 2015). Nevertheless, the new data concerning the evolution of a vapor rich fluid at low pressure and high temperature in the Banska Štiavnica stratovolcano complex (e.g. Koděra et al., 2014) indicate that such fluid/melt complexes, related to the H₂O-NaCl-KCl-FeCl₂ system, could be responsible for the formation of a new porphyry Au deposit type (Kozák et al., 2017). If so, perhaps the highest homogenization temperature recorded at Deva porphyry Cu-Au-Mo deposit (e.g. Pintea, 2014) is representative for the boiling points of the common chloride salt, NaCl (1440°C) and KCl (1411°C), representing an internal artifact of the hydrosaline melt phase without any geological meaning in that context.

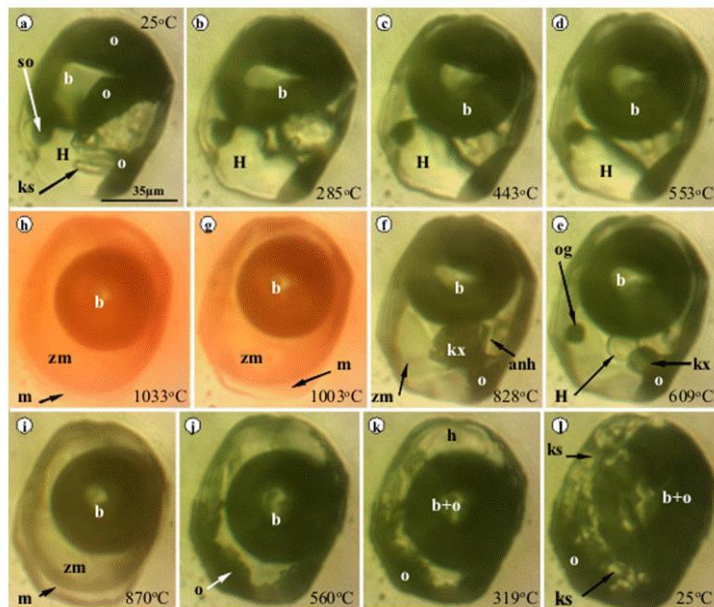


Fig. 10. Microthermometry of halite in a presumed heterogeneous hydrosaline melt inclusion from Valea Morii porphyry Cu-Au (Mo) deposit. Notations: so- solid opaque, H- halite, o- another opaque, b- bubble, ks- soluble minerals, og- globular opaque (liquid), anh- anhydrite, zm- hydrosilicate liquid, m- silicate melt. Scale bar: 35µm.

Homogeneous trapping is characteristic of hydrosaline melt inclusions which become “single-phase state” at vapor bubble homogenization and could be representative for a specific homogeneous population of inclusions or a part of a heterogeneous brine inclusion assemblage which trapped various proportion of fluid/melt phases. As an example, in Fig. 11 a homogeneous hydrosaline melt inclusions indicated $T_{mH} = 554^{\circ}\text{C}$, and $T_{bubble} = 889^{\circ}\text{C}$. The SoWat calculated pressure is $P = 1246.21$ bar, salinity is $W_s = 67.5962$ wt% NaCl eq., and density $d = 0.773078$ g/ccm, and the fluid is in the single-phase state (homogeneous). The vapor bubble renucleated at $T_{bubble} = 778^{\circ}\text{C}$, halite suddenly formed at $T_{nH} = 538^{\circ}\text{C}$ and ultimate phases renucleated at $T_n = 207^{\circ}\text{C}$, suggesting the presence of a zeolite phase as the final product of hydrosilicate fractionation, as it could be seen in the quartz-hosted microvein system, mentioned by Stefanova et al. (2014) at Elatsite porphyry Cu-Au deposit in Bulgaria.

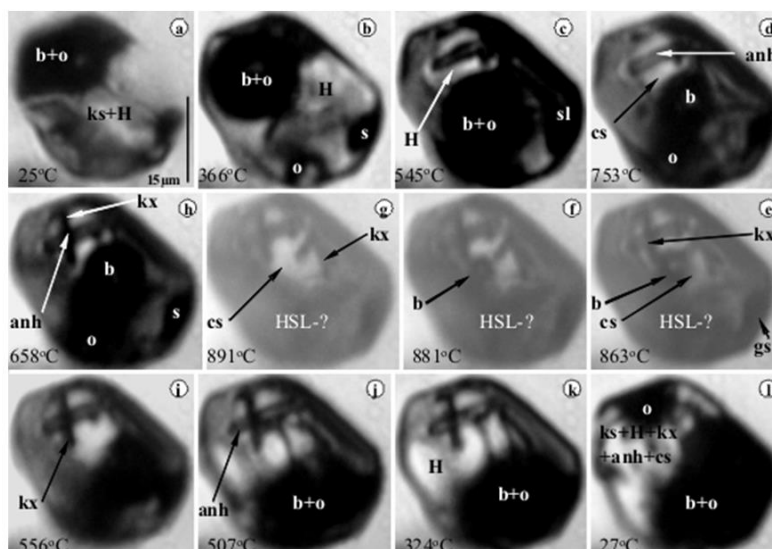


Fig. 11. Microthermometric sequences in homogeneous hydrosaline melt inclusions in quartz from Valea Morii porphyry Cu-Au (Mo) deposit. Notations: b+O- bubble+opaque, ks- saline daughter phases, s- sulfide, sl- liquid sulfide, anh- anhydrite, kx- unknown phase, cs- clathrasil (?), gs- globular sulfide. Scale bar: 15µm.

Generally, all daughter minerals melted in the presence of the vapor bubble, although frequently, some solid grains remain undissolved at the bubble homogenization temperature probably because of modifications after entrapment. It is worth noting that, at high temperatures, the final fluid is not only a simple saline mixture but rather a hydrosilicate complex liquid probably as a colloidal solution from which the melted phases renucleated due to the contraction of the silicate gel (silicothermal fluid) during quenching (Pirajno, 2009). It is assumed by experimental evidence that a separate SiO₂-rich clathrasil complex (Momma, 2014) or “a coarsened solid phase” is formed after trapping (Kotel’nikova and Kotel’nikov, 2010), and never remelted again during microthermometry, suggesting that the initial composition of the hydrosilicate liquid is now drastically changed. As a primary consequence, it is obvious that the H₂O-NaCl is only a good proxy for the complex hydrosilicate phase, which would be better characterized in the SiO₂-H₂O-NaCl system (Bodnar et al., 1985) or even better with Na₂SO₄-H₂O-SiO₂ (Kotel’nikova and Kotel’nikov, 2010), if we consider anhydrite as a real daughter phase and the presence of silicate compound as clathrasil, indicating oversaturated hydrosilicate-chloride rich phase, and indeed some of the last renucleated phases in hydrosilicate melt inclusions are zeolite-like. Probably, the same process took place in the veinlets fissure or pockets generating alteration-mineralization assemblages in the potassic and phyllic zones (see also Stefanova et al., 2014). The white coarsened solid component (i.e. clathrasil) is a ubiquitous “relic” in the Miocene porphyry Cu-(Au-Mo) system from Metaliferi Mountains but is also in the Upper Cretaceous porphyry Cu-(Mo-Au) in the Banat region and in pegmatites from Vlădeasa granite in the North Apuseni Mountains.

It has been known for a long time (e.g. Cloke and Kesler, 1979; Sterner and Bodnar, 1987; Campbell et al., 2001; Becker et al., 2008; Lecumberri-Sanchez- et al., 2012) that in many natural and synthetic compositions of the H₂O-NaCl system, the halite dissolution temperature is higher than the vapor bubble homogenization temperature (Fig. 12) or sometimes these are equal. In Fig. 12 the vapor bubble disappeared before halite dissolution in complex hydrosaline melt inclusion from Talagiu porphyry Cu-Au-Mo deposit from Metaliferi Mountains (Miocene) in South Apuseni Mountains (western Romania). SoWat calculates, for final halite homogenization temperature T_{mH}= 599°C and bubble disappearance temperature T_{hbubble}= 512°C, a pressure of P= 1628.25 bar, salinity W_s= 72.5583 wt% NaCl eq., and density d= 1.33906 g/ccm, with NaCl molecular fraction x= 0.4; the fluid is “single-phase state”.

Such microthermometric behavior leads to various theoretical and practical explanations such as the following: 1. these inclusions are accurate geobarometers (e.g. Roedder and Bodnar, 1980), or 2. their microthermometry is influenced by the entrapment mode which includes, by textural evidence, that halite was trapped together with the liquid phase as a heterogeneous suspension leading to “the potential to overestimate the fluid inclusion salinity” (Campbell et al., 2001). Moreover, “it appears that much of the published data for fluid inclusions that homogenize by halite dissolution represent inclusions that have either trapped a halite crystal along with the liquid or have reequilibrated by necking and/or stretching” (Becker et al., 2008). An interesting issue in this context is the “salting out” effect (Hovland et al., 2014) which preclude that halite particle forms at the supercritical condition at around 400°C or more function of the salinity of the H₂O-NaCl system, and they could easily be trapped as solid particle together with some liquid phase in the inclusion cavity.

5.2. Anhydrite microthermometry

Anhydrite is another common daughter solid phase present in almost all hydrosaline melt inclusions from the porphyry copper and pegmatites from Metaliferi Mountains (Miocene), Banat region and North Apuseni Mountains (Upper Cretaceous), respectively. It appears in short or longer prisms (baguette) with high birefringence and characterized by a large range of melting temperatures, depending on the global composition of the hydrosaline melt inclusion. Despite the fact that it is so common in porphyry copper systems, there are few data on anhydrite microthermometry mainly because of the complexity of brine inclusions making it hard to be observed directly under the microscope heating stage.

During heating, generally, anhydrite is more easily visible after the halite dissolution (see also Braxton, 2007) when it appears as long prismatic, baguette, next to the vapor bubble, and sometimes a silicate phase (mica) and one or more opaque grains (sulfide and oxide) are present too. On further heating, it disappeared before vapor bubble homogenization (e.g. Fig. 13) and their melting temperature almost fits the experimental data in the Albite-Quartz-Anhydrite-H₂O system (Ducea et al., 1999). In Fig. 13 the melting temperatures are the followings: T_{m1}= 66-238°C, T_{mH}= 543°C, T_{manh}= 723°C, vapor bubble disappearance temperature in the presence of liquid opaque phase at T_{hbubble}= 770°C. It is shown that at T_{max}= 1062°C in the stage the opaque liquid is still there but his diameter decreased substantially.

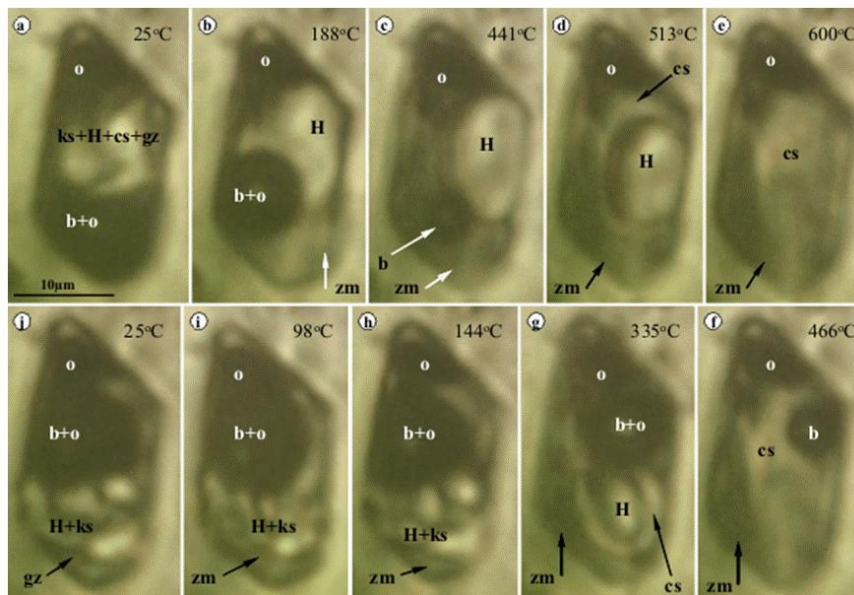


Fig. 12. Brine inclusion microthermometry by halite homogenization in quartz from Tălagiu porphyry Cu-Au (-Mo) deposit. Notations: ks- soluble salt, H- halite, cs- clathrasil, b- bubble, o- opaque, zm- hydrosilicate liquid (melt), gz- transparent glassy coverage. Scale bar: 10µm.

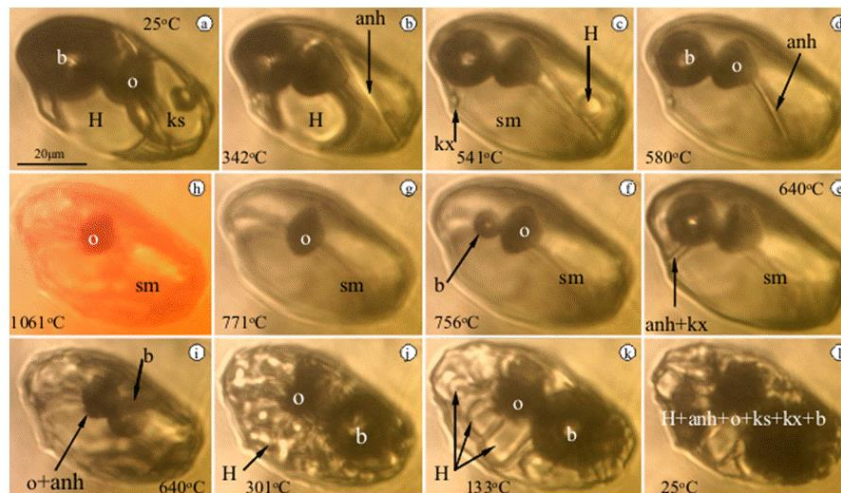


Fig. 13. Anhydrite microthermometry in a homogeneous hydrosaline melt inclusion in quartz from Roşia Poieni. Notations: b- bubble, o- opaque, H- halite, ks- other salt daughter minerals, anh- anhydrite, kx- unidentified phase. Scale bar: 20µm.

Trapping conditions calculated by SoWat at 770°C, give: pressure, $P=907.48$ bar, salinity, $W_s=66.0109$ wt % NaCl eq., and density, $d=1.064$ at NaCl mole fraction, $x=0.4$. Originally the fluid is in the “single-phase state”. On quenching, anhydrite renucleated after the vapor bubble and before halite renucleation. Generally, the microthermometric cycles were reproducible. Although, for example in a batch of hydrosaline melt inclusions ($n=102$) from Valea Morii porphyry Cu-(Au)-(Mo) deposit (Pintea, unpublished data) even though anhydrite was always present, only in 23 cases from 102 microthermometric analyses (as an example), anhydrite melting temperature was recorded between 803°-1063°C. During quenching, anhydrite renucleated between 658°-793°C, but the process is very difficult to be recorded and, unfortunately, this could only be observed in 4 microthermometric analyses of the same batch of measurements. Nevertheless, many repeated microthermometric analyses from the batch samples mentioned above, have shown again, after quenching, the presence of anhydrite, so it is a matter of optical microscopy determination of the tiny anhydrite microcrysts rather than the absence of anhydrite daughter phase. Perhaps by coupling Raman spectroscopy during microthermometry the anhydrite could be better evidenced, as it is presumed after several cycles of the same inclusion from Fig. 13, by the characteristic peak at 983 cm^{-1} which is indicative for the presence of (SO_4^{2-}) by very strong molecular vibrational stretching (e.g. Arcanite – K_2SO_4 , Frezzotti et al., 2012, in Fig. 14).

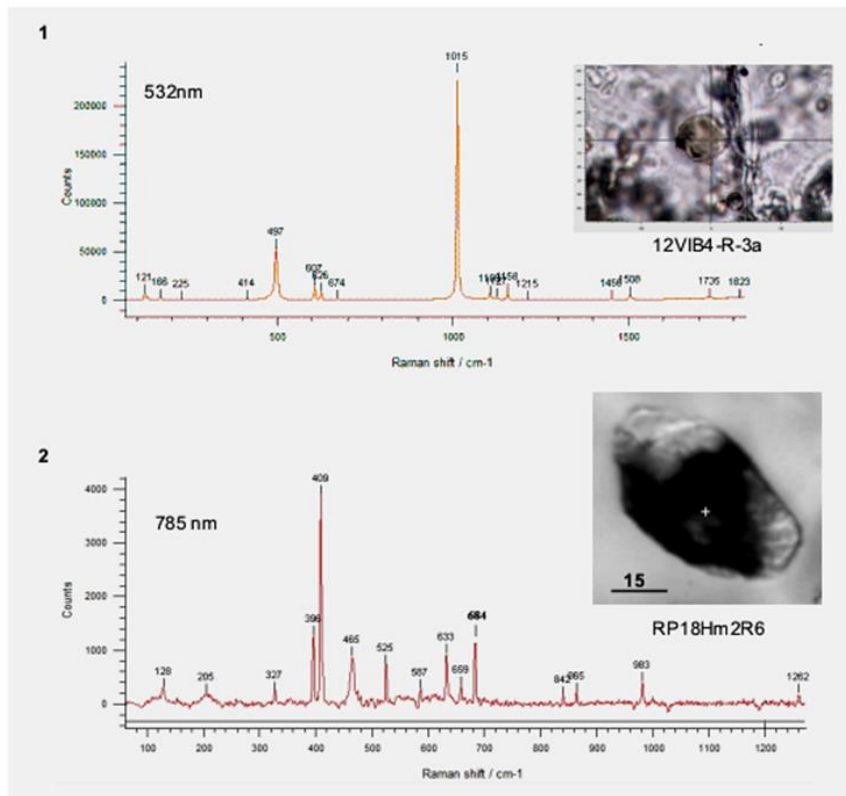


Fig. 14. Solid inclusion (glassy) in quartz from Voia porphyry Cu-Au-Mo deposit before microthermometry indicating the vibrational stretching of anhydrite at 1015-1016 cm^{-1} (Burke, 1994), in (1), and the Raman spectra in the same inclusion from Fig. 13 after microthermometry (scale bar: 15 μm). The Raman shift peaks are indicative for sulphate (983 cm^{-1}), carbonate (1081 cm^{-1}), hematite (409 cm^{-1}), ilmenite 684 cm^{-1} , sulfide (<400 cm^{-1}), in (2).

5.3. Opaque phases microthermometry

The alteration-mineralization stages in porphyry copper genesis are composed mainly by the veinlets and brecciated zones dominated by magnetite, hematite (specularite), chalcocopyrite, pyrrhotite, sulfosalts, pyrite, marcasite, all of which are associated with quartz, anhydrite, gypsum, calcite, and sometimes fluorite and alunite. Many of these minerals were also formed in hydrosaline melt inclusions after sealing in the host minerals (mostly studied in quartz).

One of the most important observations is that after (sometimes before) halite dissolution, the opaque minerals (oxides, sulfides) become globular most probably in the liquid state and most probably turning into chloride compounds before they were homogenized in the hydrosilicate-salt liquid. Moreover, some of these (typically oxides) are attached to the vapor bubble until they are completely melted around the bubble disappearance temperature. That is, at high temperature, magnetite is floating together with the vapor phase in the hydrosaline melt inclusions.

5.3.1. Magnetite/hematite

Magnetite is one of the common opaques in hydrosaline melt inclusions and generally, during heating, a sudden transition was observed above 650°-700°C changing them to transparent platelets of hematite or FeCl_2 (Pintea, 2009). On further heating, these new phases become rounded and are perhaps in a liquid state as iron chloride, dissolving at very high temperatures (Pintea, 2014).

It was noted that during the heating/quenching microthermometric cycles, the oxide minerals and even sulfides are in very close relationship with the vapor bubble evolving together during temperature variations. This phenomenon is very common at the large scale in the subvolcanic-magmatic system where during degassing, sulfides and magnetite are attached to the vapor bubble and transported despite gravity forces at the surface and precipitated as individual layers (Edmonds, 2015; Mungall et al., 2015; Knipping et al., 2019). In Fig. 15 the microthermometry indicates that the halite melted at $T_{\text{mh}} = 464^\circ\text{C}$ and the homogenization temperature is more than 1081°C. The SoWat estimated a pressure of $P = 2331.66$ bar, the salinity, $W_s = 55.0043$ wt% NaCl eq., and density, $d = 0.883646$ g/ccm with NaCl molar fraction, $x = 0.27$. As it is confirmed, the fluid is in the (V+L) state, because the homogenization temperature cannot be reached in our microthermometric stage. So, probably the initial state of the fluid was

homogeneous above 1081°C. An unknown transparent phase melted at $T_{\text{mds}} = 716^\circ\text{C}$, the opaque melted between 936°C - 1025°C , which renucleated at 644°C . The unknown transparent phase (ds) renucleated at 609°C . Anhydrite melted above 936°C . In 16 out of 102 microthermometric analyses of hydrosaline melt inclusions at Valea Morii deposit, as mentioned above, the opaque phase is presumed to be a magnetite/hematite daughter phase, and the melting temperature ranged between 786°C - 1068°C . The renucleation process showed the formation of similar opaque phases but they are difficult to be microscopically identified even by Raman spectroscopy. Anyhow, the high melting temperatures indicate that magnetite/hematite has formed inside the hydrosaline melt or hydrosilicate melt inclusions after trapping, indicating a magmatic or hydrothermal origin as it was demonstrated by silicate melt inclusion in magnetite microthermometry (Knipping et al., 2015) and by exsolution from iron-rich melt at the El Laco magnetite lava flows (Tornos et al., 2016).

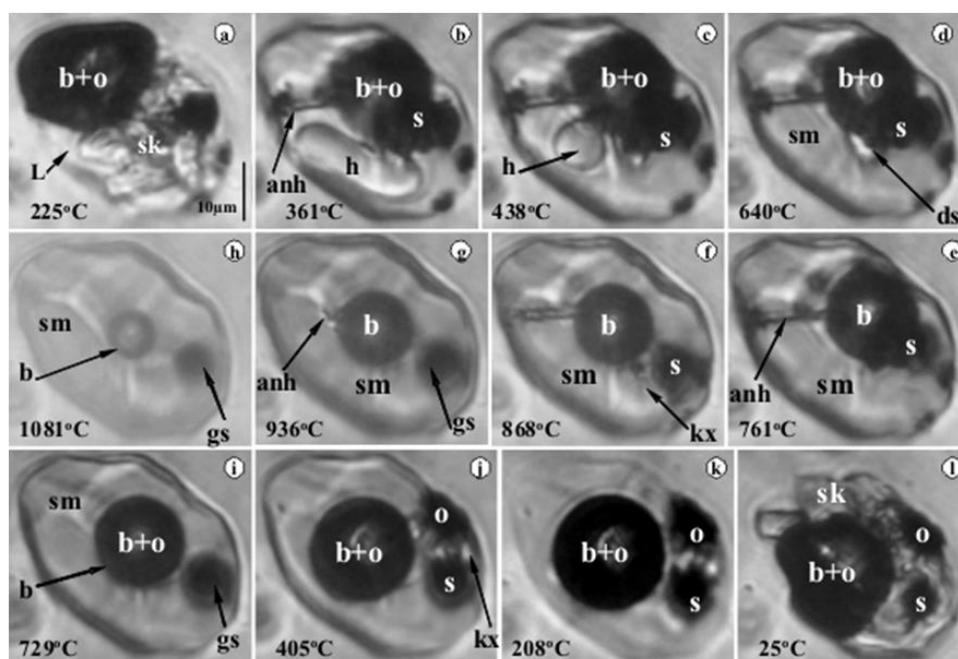


Fig. 15. Microthermometric sequence in heterogeneous hydrosaline melt inclusion in quartz from Bolcana porphyry Cu-Au (Mo) deposit. Notations: sk- salt crystals, b- bubble, ds- unknown solid phase, anh- anhydrite, o- oxide (magnetite and/or hematite), sm- salt melt, gs- globular liquid sulfide, kx- unknow solid. Scale bar: $10\mu\text{m}$.

5.3.2. Triangular chalcopyrite microthermometry

Besides optical microscopy, SEM-EDS, PIXE, or direct chemical analysis, the presence of triangular chalcopyrite as a truly daughter phase can be proved by coupling microthermometry with Raman spectroscopy (Fig. 16 and Fig. 17). It is well known that chalcopyrite is consistently present in hydrosaline melt inclusions from porphyry copper deposits since the fluid and melt inclusion assemblages of these deposits have been extensively investigated (e.g. Roedder, 1971, 1984; Nash, 1976; Eastoe, 1978; Ramboz, 1979; Lowenstern, 1993; Damman et al., 1996; Redmond et al., 2004; Heinrich et al., 2005; Kouzmanov and Pokrovski, 2012).

It is also observed that chalcopyrite obviously doesn't melt during heating in low salinity vapor-rich inclusions, mainly because of the H_2 moving in or out after entrapment (Mavrogenes and Bodnar, 1994; Spencer et al., 2015). Moreover, some recent experimental work demonstrated that several elements such as Cu, Ag, Na can diffuse out or in, inducing important modification of the initial fluid and melt inclusion content (Li et al., 2009; Lerchbaumer and Audéat, 2012; Seo and Heinrich, 2013). Nevertheless, "Sterner and Bodnar (1984) showed that by adding a large excess of powdered chalcopyrite to capsules containing 10 wt% NaCl solution, inclusions containing chalcopyrite daughter mineral were produced. When these inclusions are heated, the chalcopyrite completely dissolves and reprecipitates when the inclusions are cooled" (Bodnar and Sterner, 1987). The same successful chalcopyrite microthermometry was achieved by using the hydrogenation technique proposed by Mavrogenes and Bodnar (1984), which was perfected recently by Spencer et al. (2015). In both experimental studies, chalcopyrite proved to be a real daughter phase by specific melting and renucleation behavior during heating/quenching cycles.

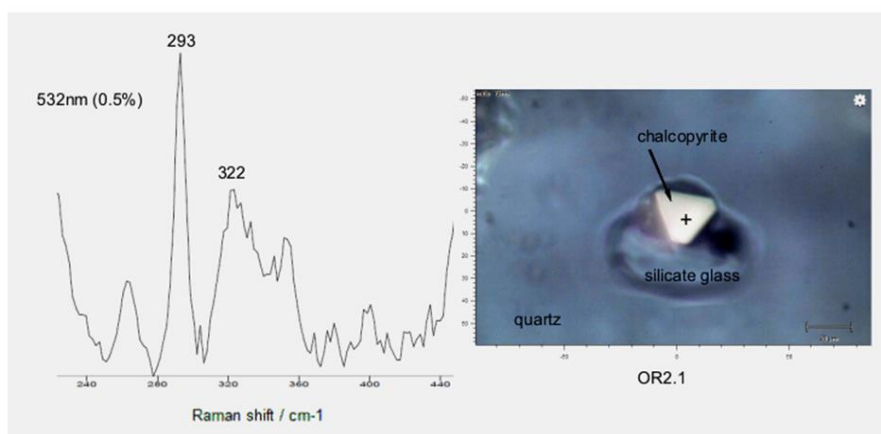


Fig. 16. Raman spectra of chalcopyrite daughter mineral in hydrosilicate melt inclusion in quartz from Oravița porphyry Cu-Mo-Au deposit (Upper Cretaceous). Chalcopyrite has a very strong peak at 293 cm^{-1} , and some weaker peaks at 322 cm^{-1} , 352 cm^{-1} and 378 cm^{-1} (Frezzotti et al., 2012). Scale bar: $25\mu\text{m}$.

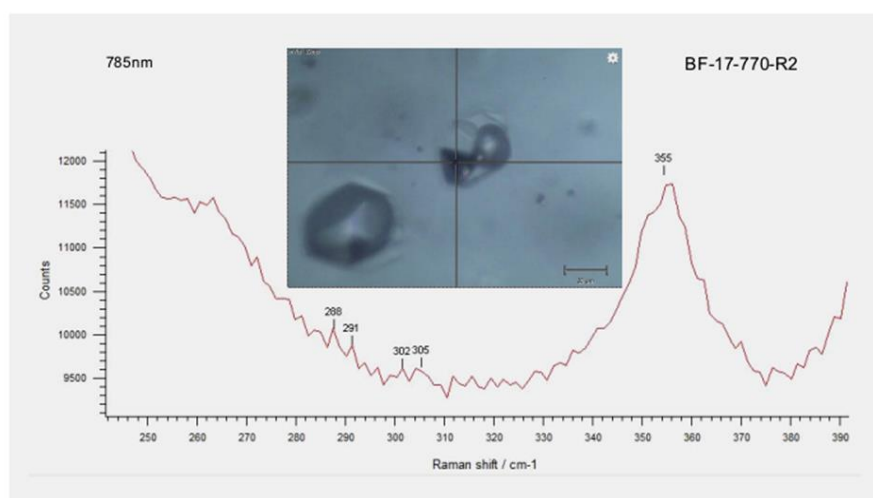


Fig. 17. Raman spectra of triangular chalcopyrite daughter mineral in hydrosaline melt inclusion of quartz from Bolcana porphyry Cu-Au-Mo deposit (Miocene). Common Raman shifts peaks between $291\text{--}293\text{ cm}^{-1}$, $320\text{--}323\text{ cm}^{-1}$, depending on laser line power and position of the inclusion in the host quartz. Scale bar: $20\mu\text{m}$.

During heating of hydrosaline melt inclusions (here as an example) the first melting temperature is given by dissolution of an intermediate complex such as iron hydrate sulfate and/or carbonate (or zeolite), together with the thin amorphous hydrosilicatic film (Pintea et al., 2018) followed by another complex phase such as javorieite (KFeCl_3) or other similar phases (e.g. Kozák et al., 2017) until halite melted sharply at 611°C , as shown in Fig. 18. At that temperature, the remaining phases are the vapor bubble and two opaque grains, one attached to the bubble and other somewhere nearby, together with a transparent baguette presumed to be anhydrite. The opaque globule attached to the vapor bubble turned to an opaque liquid globule and stayed attached until high temperature, and then it suddenly separated from the vapor bubble. At this temperature (i.e. 1050°C), an opaque globule and a vapor bubble are floating in the hydrosaline-silicate liquid. After the heating was stopped, the liquid globule immediately moved back towards the vapor bubble and started to crystallize as a thin opaque plate from inside the bubble. On further quenching, another opaque phase renucleated (oxide) together with the transparent baguette (anhydrite). The sulfide became more triangular in shape, suggesting chalcopyrite, as also revealed by the Raman shift at 291 cm^{-1} , measured several months after the microthermometry. The halite renucleated suddenly as several separate grains, which coagulated by Ostwald ripening. The last formed solid phases filled up the interstitial space between vapor, halite and the opaque phase, perhaps as a solid fragile amorphous hydrosilicatic crust (Pintea et al., 2018). Repeated microthermometric cycles followed almost the same phase transition succession and the data in Fig. 18 are compiled from them, as follows: halite melt at $T_{\text{mH}} = 611^\circ\text{C}$, the opaque phase at $T_{\text{mO}} = 1017^\circ\text{C}$, and final homogenization temperature around $T_{\text{h}} \geq 1052^\circ\text{C}$. Anhydrite melting temperature was recorded only in the second cycle, at 987°C . An unknown solid phase melted around 1040°C , and if the temperature of formation is estimated at 1052°C ,

the SoWat estimated pressure is $P= 1364.37$ bar, salinity is $W_s= 75.8046$ wt% NaCl eq., and density $d= 1.09793$, with NaCl molar fraction $x= 0.5$. The original fluid was in the “single-phase state” even if in reality the final homogenization temperature was not recorded in this case. During quenching, the opaque (chalcopyrite) renucleated at $T_{no}= 657^\circ\text{C}$ and halite renucleated at $T_{nH}= 495^\circ\text{C}$. Anyhow, the cycles are not completely reproducible due to post-entrapment modifications but because the content and number of phase transitions are almost the same in the repeated cycles it is assumed that the complex salt phase, halite, anhydrite, magnetite/hematite, chalcopyrite are daughter minerals and were precipitated from a complex hydrosaline-silicate liquid, as hydrosilicate gel or silicothermal fluid.

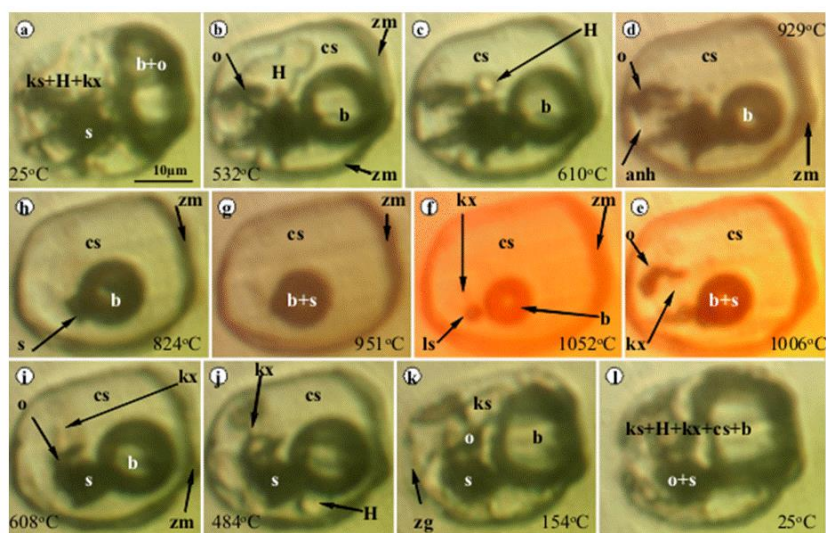


Fig. 18. Chalcopyrite melting and renucleation in homogeneous hydrosaline melt inclusion from Valea Morii porphyry Cu-Au (Mo) deposit. Notations: s- sulfide (chalcopyrite?), ls- liquid sulfide, H- halite, ks- other salts, b- bubble, cs- clathrasil (?), zg- hydrosilicate glass, o- opaque. Scale bar: 10µm.

6. Characterization of the decrepitated mound by Raman spectroscopy

During microthermometric cycles of a quartz sample, many of the hydrosaline melt inclusions decrepitated and liberated the highly concentrated liquid melt outside microcavities wetting the surface of the host mineral (i.e. quartz). These fluids precipitated obviously in a concentric microtexture with oxide/sulfide close to the micro-pit, then silicate melt and salt to the rim. So, the content of exploded inclusion is almost completely saved in this process and can be qualitatively analyzed by Raman spectroscopy. Some examples of Raman spectra are shown in Fig. 19 and Fig. 20, suggesting the presence of the main silicate, sulfide/oxide and salt minerals in inclusions before decrepitation. In fact, only the vapor phase is missing from the initial chemical composition. We also emphasized that some of the components suffered chemical modification after decrepitation caused by decompression and changing temperature, but they give important clues about the chemistry of the included fluid or melt phases. The Raman spectra show that these precipitated assemblages contain halite ($353\text{-}355\text{ cm}^{-1}$), silicate glass ($628\text{-}633\text{ cm}^{-1}$), hematite (409 cm^{-1}), chalcopyrite ($291\text{-}293\text{ cm}^{-1}$), magnetite (654 cm^{-1}), other sulfides ($<500\text{ cm}^{-1}$), sulfate (983 cm^{-1}), carbonate ($1028\text{-}1081\text{ cm}^{-1}$) and phosphate ($916\text{-}1000\text{ cm}^{-1}$) ions, comparative to the data from RRuff Raman database, Frezzotti et al. (2012) and Hurai et al. (2015). The concentric deposition of the precipitate is interesting, suggesting immiscibility even during quenching at the surface of the host-quartz sample. Anyhow, there are some notable variations, as a function of the inclusion types suggesting that each micro-pit contains its specific initial chemical composition, and perhaps other unknown causes, and the Raman spectra of this study should be interpreted only as qualitative and informative.

7. Discussion

Based upon several hundreds of microthermometric measurements on hydrosaline melt inclusions from the Miocene of the Metaliferi Mountains, Eastern Carpathians and the Upper Cretaceous porphyry Cu-(Mo)-(Au) deposits in the Banat region and pegmatites from Vlădeasa granite massif in the North Apuseni Mountains, Pinteá (1993; 1997; 2002; 2009; 2012; 2014) it has been shown that there are at least four types of partial homogenization to one or more liquids as follows: **1.** complex silicate melt - hydrosaline melt inclusions showing silicate melt-salt melt assemblages at partial homogenization

temperature $T_{hp} = 1100^\circ$ to $> 1300^\circ\text{C}$ by vapor bubble homogenization in the salt melt fraction; **2.** hydrosaline melt inclusions without visible liquid solution at room temperature conditions, forming a salt melt and silicate melt immiscible mixture between 1000° to $>1200^\circ\text{C}$ by bubble disappearance in the salt melt globule; **3.** hydrosaline melt inclusions with some aqueous liquid fraction generating salt melt \pm silicate melt rim \pm unmelted solid phases after vapor bubble homogenization between 700° to 1000°C ; and **4.** brine inclusions with a larger aqueous liquid fraction homogenizing by vapor bubble or halite disappearance at temperatures between 450°C (or lower especially in the Upper Cretaceous samples) to less than 700°C - 800°C .

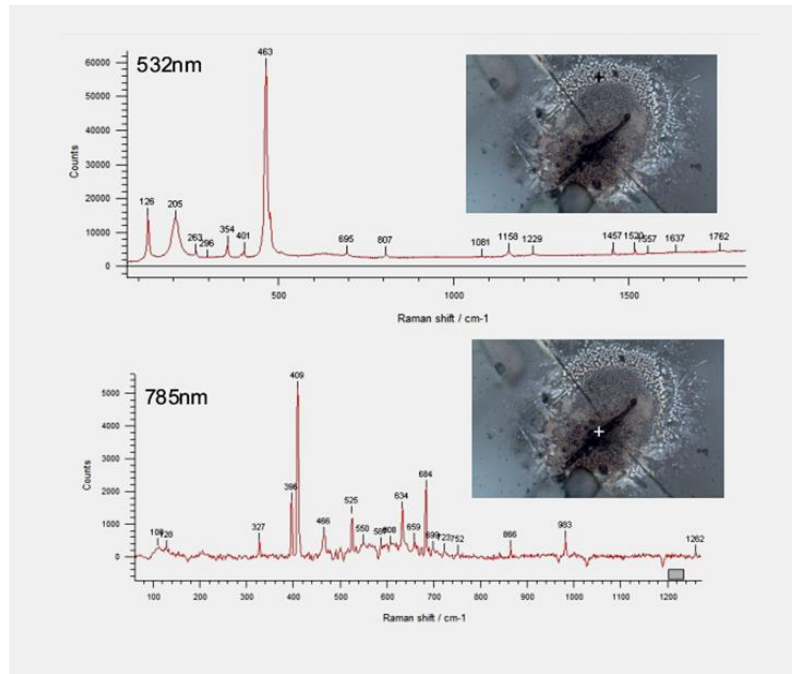


Fig. 19. Raman spectra of the decrepitated mound precipitated concentrically around the former hydrosaline melt inclusion in quartz from Roşia Poieni porphyry Cu-Au-(Mo) deposit. (see text for explanations).

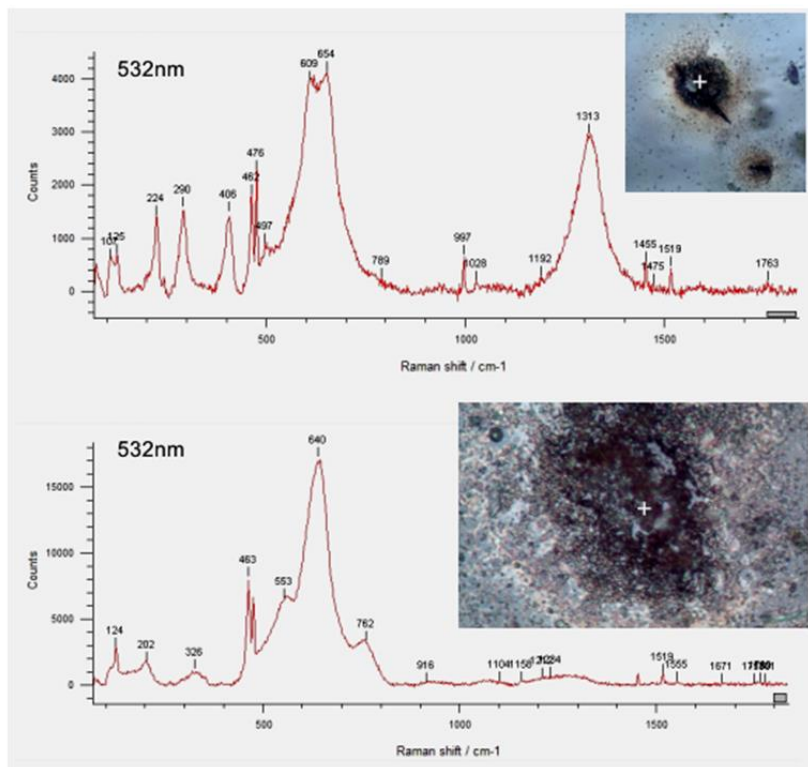


Fig. 20. Raman spectra of decrepitated mound precipitated around the former hydrosaline melt inclusion in quartz from Bolcana porphyry Cu-Au-(Mo) deposit (see text for explanations).

By fixing the formation temperature at around 1085°C based upon the beginning of the silicate liquid formation in hydrosaline melt inclusions and salt melt exsolution in the contemporaneous silicate melt inclusions in the same assemblage (Pintea, 1995, 1996b, 2007, 2009, 2014), it is rational to compare these entrapment conditions to the Burnham model (1979) of granodioritic magma crystallization as a primary source of fluid and ore elements (protore) in porphyry copper genesis (Bodnar, 1995; Becker, 2008, Bodnar, 2010). That is a dynamic fluid-melt system sourced at the bottom of the magma chamber by successive basic influxes especially with a volatile-rich front interacting with felsic mushes above. The main porphyry stock formation contains representative quartz veinlets in successive cross-cutting relationships with potassic and phyllic mineralization–alteration facies (e.g. Sillitoe, 2010). This means that the melting/renucleation temperatures of the solid daughter phases determined by microthermometry coupled with Raman spectroscopy in this study suggest successive fluid-melt fractionation during decompression and changing temperature. This happens during the transition from the magmatic to hydrothermal stages in the presence of a hydrous silicate melt (silicothermal fluid) which segregates chlorides, sulfides, sulfates, oxide phases, and partitions the ore elements by immiscibility and boiling episodes.

Similar results were published recently by Mernagh and Mavrogenes (2019) for the Grasberg porphyry Cu-Au deposit, especially the case of their defined B2 hydrosaline melt inclusion in quartz paragenesis, which is similar to the hydrosaline inclusions in porphyry copper systems in Romania (e.g. Pintea, 2014). By coupling microthermometry with LA-ICP-MS, their study has shown the chemical complexity of these high-temperature inclusions containing Na (20-60 wt%), K (20-40 wt%, occasionally up to 70 wt%) and Fe (20-50 wt%) as major elements and lower amounts of Li, Mg, Al, S, Ca, Ti, Cu, As, Se, Rb, Sr, Y, Mo, Cs, Ce, Yb and Pb. The majority of these components are transported initially as chloride and sulfide/oxide complexes and they melted and recrystallized “in situ” during heating/quenching microthermometric cycles.

There is now important evidence on the presence of FeCl₂-KCl-NaCl in hydrosaline melt inclusions and other fluid inclusion types (Koděra et al., 2014; Mernagh and Mavrogenes, 2019) together with H₂O-NaCl (Bodnar et al., 1985), H₂O-CaSO₄ (Kotel'nikova and Kotel'nikov, 2010, 2016), H₂O-CaCO₃ (Kotel'nikova and Kotel'nikov, 2011) evolving from a hydrosilicate liquid (Smirnov et al., 2017) in various P-V-T-X conditions. In our study, they form at temperatures of about 1085°C, the pressure ranges from less than 100 bar up to more than 2kb, and the salinity from 30 wt% to more than 70-80 wt% NaCl eq. It is worth mentioning that hydrosilicate liquid behaves as a colloidal solution or silicothermal fluid-melt emulsion (e.g. Pirajno, 2009; Wilkinson et al, 1996; 2015; Thomas and Davidson, 2016; Pintea et al., 2018) from which chloride melt, sulfide and oxide segregated by immiscibility and successive boiling episodes during decompression and temperature changes. Around 100 Raman spectra on hydrosaline and vapor-rich melt inclusions from porphyry Cu-Au-Mo deposit in both regions mentioned above, suggest the presence of CO₂, CO₃²⁻, HCO₃⁻, SO₄²⁻, PO₄³⁻, and the molecular vibration modes of S-H, C-H and O-H could be assigned to H₂S, CH₄, CO₂ and H₂O as main volatile phases partitioned between silicate melt and aqueous fluid. The latest ones were already measured quantitatively by Gas Chromatography – Mass Spectrometry in the Miocene porphyry Cu-Au deposit from the Metaliferi Mountains (Pintea, 1996; Cuna et al., 2001);

8. Conclusions

Complementary microthermometry and Raman spectroscopy data in this study on silicate melt and hydrosaline melt inclusions from Upper Cretaceous and Miocene porphyry Cu-(Au)-(Mo) deposits from the Banat region and the South Apuseni Mountains (Metaliferi Mountains) confirmed the previously published data and observations (Pintea, 2014, and references therein), indicating the complexity of the PVTX trapping conditions in these deposits. Many of the included phases are truly daughter mineral phases formed from a complex hydrosilicate liquid mainly by fluid-melt immiscibility.

The most important successive phase transitions are the following:

A. Heating melting temperatures:

1. Hydrous compounds or other solid complexes including sylvite (~70°-300°C);
2. The second melting points (~300°-350°) of solid complexes such as javorieite (KFeCl₃ - Koděra et al., 2017);
3. Halite melting temperature (468°-662°C), the main T_m reference for salinity estimation;
4. Magnetite and/or hematite turning to hematite and/or FeCl₂ or an opaque liquid phase, respectively (786°-1068°C);
5. Anhydrite final dissolution temperature (723°-1063°C) in hydrous salt-silicate melt association;

6. Vapor-rich “melt” bubble (Vm) dissolution temperature at the final homogenization temperature (Th) or sulfide-salt-silicate immiscible final phase state (682°-1426°C, Pintea, 2014).

B. Main quenching temperatures are the following:

1. Sudden Vm (i.e. vapor-rich “melt”) renucleation (1284°-659°C, Pintea, 2014);

2. Opaque phase recrystallization (845°-681°C);

3. Anhydrite renucleation (658-793°);

4. Chalcopyrite precipitation (650°-500°C);

5. Halite renucleation (574°-255°C);

6. Another opaque and transparent phase formation (less than 200°C).

It is worth noting that during heating/quenching cycles the opaque phases and other saline/silicate/sulfate compounds remain in a liquid state over a large temperature interval. However, the microthermometry cycles are not always reproducible mainly because of “in-situ” modifications, during heating-cooling especially for chalcopyrite (see also Spencer et al., 2015). Anyhow, the high-temperature microthermometry in silicate-, and hydrosaline melt inclusions coupled with Raman spectroscopy give the following valuable information on P-T-X properties of the initial enclosed fluid/melt phases:

- during the heating procedure at least two (or three) liquid (melt) phases are coexistent around the proposed entrapment temperature suggesting immiscibility and/or heterogeneous trapping;
- on quenching, a vapor-rich “melt” is suddenly renucleated followed by the recrystallization of sulfates, oxides, silicates, sulfides and saline daughter microphases. Frequently, a coarsened solid phase, presumably a “clathrasil” compound, is precipitated after trapping and never remelts during additional microthermometry. Its presence suggests that initially the hydrosaline melt inclusions were more silica-rich and they were obviously heterogeneously trapped;
- the Raman spectroscopy suggests the presence of CO₂, CO₃²⁻, HCO₃⁻, SO₄²⁻, PO₄³⁻, and the molecular vibration modes of S-H, C-H and O-H could be assigned to H₂S, CH₄, CO₂ and H₂O as main volatile phases partitioned between silicate melt and aqueous fluid;
- the complex fluid phase assemblages exsolved from deep MASH zones, where the parental melt originated and mixed again at shallow levels with silicate crystal mushes, are the precursors of mineralized high temperature potassic and phyllic alteration zones in Alpine porphyry Cu-(Au)-(Mo) deposits from Romania.

Acknowledgements. The study has been partially supported by the Research Projects no. PN19-45-01-02 financed by the Romanian Ministry of Research and Innovation, and no. 29 PCCDI/2018 “GEORES” and PN-III-P4-ID-PCCF-2016-4-0014 “CUTE” financed by UEFISCDI, Romania. Many thanks to Dr. T. Mernagh for valuable criticism improving substantially the manuscript.

References

- Audétat A., Simon A.C. (2012) Magmatic controls on porphyry copper genesis. Soc. Econ. Geol., Inc., Spec. publ., 16, p. 553-572.
- Bakker R.J. (2003) Package FLUIDS 1. Computer programs for analysis of fluid inclusion data and for modelling bulk fluid properties. Chem. Geol., 194, p. 3-23.
- Becker S.P. (2007) Fluid inclusion characteristics in magmatic-hydrothermal ore deposits. PhD thesis, Virginia Polytechnic Inst. and State Univ., Blacksburg, VA, USA, 138p.
- Becker S.P., Fall A., Bodnar R.J. (2008) Synthetic fluid inclusions. XVII. PVTX properties of high salinity H₂O-NaCl solutions >30 wt% NaCl: application to fluid inclusions that homogenize by halite disappearance from porphyry copper and other hydrothermal ore deposits. Econ. Geol. 103, p. 539–554.
- Berbeleac I., Udubaşa S.S., Iatan E.L., Vişan M. (2014) Geological and structural constraints on the localization of Neogene porphyry-epithermal related Cu-(Au)-(Mo), and epigenetic hydrothermal deposits/prospects from South Apuseni Mts., Romania. Rom. J. Miner. Deposits, 87/1, p. 47-52.
- Blundy J., Mavrogenes J., Tattitch J.B., Sparks S., Gilmer A. (2015) Generation of porphyry copper deposits by gas-brine reaction in volcanic arcs. Nature Geosci. 8, p. 235-240.
- Bodnar R.J. (1995) Fluid inclusion evidence for a magmatic source for metals in porphyry copper deposits. Mineralogical Association of Canada, Short Course Volume 23, p. 139–152.
- Bodnar R.J. (2003) Introduction to aqueous-electrolyte fluid inclusions. In: Samson I., Anderson A., Marshall D. (eds.) Fluid Inclusions: Analysis and Interpretation. Mineralogical Association of Canada Short Course, 32, p. 81-100, Québec.
- Bodnar R.J. (2010) Magmatic fluid evolution associated with epizonal silicic plutons. ACROFI & TBG XIV, Novosibirsk, Russia, Abstr. Vol., p. 30-31.

- Bodnar, R.J., Burnham, C.W., Sterner, S.M. (1985) Synthetic fluid inclusions in natural quartz. III. Determination of phase equilibrium properties in the system H₂O-NaCl to 1000°C and 1500 bars. *Geochim. et Cosmochim. Acta*, 49, p. 1861–1873.
- Bodnar R.J., Sterner S.M. (1987) Synthetic fluid inclusions. In: Ulmer G.C. and Barnes H.L. (eds.) *Hydrothermal experimental techniques*. New York, Wiley-Interscience, p. 423–457.
- Bodnar R.J., Vityk, M.O. (1994) Interpretation of microthermometric data for H₂O-NaCl fluid inclusions. In: De Vivo B. and Frezzotti M.L. (eds.) *Fluid Inclusions in Minerals: Methods and Applications*. Virginia Tech, Blacksburg, VA, p. 117-130.
- Braxton D.P. (2007) Bayongan and Bayugo porphyry gold deposits NE Mindanao, Philippines: geology, geochemistry, and tectonic evolution. PhD thesis, Univ. of Tasmania, 277p.
- Burke E.A.J. (1994) Raman microspectrometry of fluid inclusions: the daily practice. In: De Vivo B. and Frezzotti M. L. (eds.) *Fluid Inclusions in Minerals: Methods and Applications*. Virginia Tech., Blacksburg, VA, p. 25-44.
- Burnham C.W. (1979) Magmas and hydrothermal fluids. In: Barnes H.L. (ed.) *Geochemistry of Hydrothermal ore deposits*. 2nd Ed. John Wiley, New York, p. 71–136.
- Campbell A.R., Lundberg S.A.W., Dunbar N.W. (2001) Solid inclusions of halite in quartz: evidence for the halite trend. *Chem. Geol.*, 173, p. 179-191.
- Campos E., Touret J.L.R., Nikogosian I., Delgado J. (2002) Overheated, Cu-bearing magmas in the Zaldívar porphyry-Cu deposit, Northern Chile. *Geodynamic consequences*. *Tectonophysics*, 345, p. 229-251.
- Cioacă M, Munteanu M. (2012) The present state of knowledge on the high technology elements in porphyry copper deposit from Romania. EGU General Assembly 2012, Geophysical Research Abstracts, Vol. 14, EGU2012-4402.
- Ciobanu C.L., Cook N.J., Stein H. (2002) Regional setting and geochronology of the Late Cretaceous Banatitic Magmatic and Metallogenic Belt. *Miner Deposita*, 37, p. 541-567.
- Cloke P.L., Kesler S.E. (1979) The halite trend in hydrothermal solutions. *Econ. Geol.*, 74, 8, p. 1823-1831.
- Cuna S., Palibroda N., Cuna C., Pintea I. (2001) The mass spectrometric method for analysis of volatile species from fluid inclusions. ABCD-GEODE Workshop, Vața Băi, Romania. *Rom. J. Miner. Deposits*, 79, suppl 2., p. 48-49.
- Damian F. (2003) The Mineralogical Characteristics and the Zoning of the Hydrothermal Types Alteration from Nistru Ore Deposit, Baia Mare Metallogenic District. *Studia Univ. "Babeș-Bolyai", Geol.*, XLVIII, 1, p. 101-112.
- Damman A.H., Kars S.M., Touret J.L.R., Rieffe E.C., Kramer J.A.L.M., Vis R.D., Pintea I. (1996) PIXE and SEM analysis of fluid inclusions in quartz crystals from the K-alteration zone of the Rosia Poieni porphyry Cu deposit, Apuseni Mountains, Rumania. *Eur. J. Mineral*, 8, p. 1081-1096, Stuttgart. Germany.
- Drew L.J. (2006) A tectonic model for the spatial occurrence of porphyry copper and polymetallic vein deposits - applications to Central Europe. U.S. Geological Survey Scientific Investigations Report 2005–5272, 36 p.
- Driesner T., Heinrich C. A. (2007) The System H₂O–NaCl. Part I: correlation formulae for phase relations in temperature-pressure-composition space from 0 to 1000°C, 0 to 5000 bar, and 0 to 1 X_{NaCl}. *Geochim. et Cosmochim. Acta* 71 (20), p. 4880–4901.
- Driesner T. (2007) The System H₂O–NaCl. II. Correlations for molar volume, enthalpy, and isobaric heat capacity from 0 to 1000 degrees C, 1 to 5000 bar, and 0 to 1 X_{NaCl}. *Geochim. et Cosmochim. Acta* 71(20), p. 4902-4919.
- Ducea M.N., McInnes B.I.A., Wyllie P.J. (1999) Experimental determination of compositional dependence of hydrous silicate melts on sulphate solubility. *Eur. J. Mineral.*, 11, p. 33-43.
- Eastoe C.J. (1978) A fluid inclusion study of the Panguna porphyry copper deposit, Bougainville, Papua New Guinea. *Economic Geology*, 73, p. 721–748.
- Edmonds M. (2015) Flotation of magmatic minerals. *Geology*, 43, 7, p. 655-656.
- Frezzotti M.L., Tecce F., Casagli A. (2012) Raman spectroscopy for fluid inclusion analysis. *Journ. of Geochim. Expl.*, 112, p. 1-20.
- Gallhofer D. (2015) Magmatic geochemistry and geochronology in relation to the geodynamic and metallogenic evolution of the Banat Region and the Apuseni Mountains of Romania. Diss. thesis ETH Zürich No. 22888, 145p.
- Gheorghită I. (1975) Mineralogic and petrographic study of the Moldova Nouă region Suvorov-Valea Mare zone. (In Romanian with extended English abstract). *Inst. Geol., Geofiz., Stud. Tehn. Econ., Ser. I., Min. -Petrogr.*, nr.11, 188p.
- Hack A.C., Mavrogenes J.A. (2006) A synthetic fluid inclusion study of copper solubility in hydrothermal brines from 525 to 725°C and 0.3 to 1.7 GPa. *Geochim. et Cosmochim. Acta*, 70, p. 3970-3985.
- Harris C.R., Pettke T., Heinrich C.A., Roșu E., Woodland S., Fry B. (2013) Tethyan mantle metasomatism creates subduction geochemical signatures in non-arc Cu–Au–Te mineralizing magmas, Apuseni Mountains Romania. *Earth and Planet. Sci. Lett.*, 366, p. 12-136.
- Haynes F.M., Sterner S.M., Bodnar R.J. (1988) Synthetic fluid inclusions in natural quartz. IV. Chemical analyses of fluid inclusions by SEM/EDA: Evaluation of method. *Geochim. et Cosmochim. Acta*, 52, p. 969-977.

- Heinrich C.A., Cousens D.R. (1989) Semi-quantitative electron microprobe analysis of fluid inclusion salts from the Mount Isa copper deposit Queensland, Australia. *Geochim. et Cosmochim. Acta*, 53, p. 21-28.
- Heinrich C.A., Halter W., Landtwing M.R., Pettke T. (2005) The formation of economic porphyry-gold deposits: constraints from microanalysis of fluid and melt inclusions. In: McDonald I., Boyce A.J., Buttler I.B., Herrington R.J., Polya D.A. (eds.) *Mineral Deposit and Earth evolution*. Geol. Soc. London, Spec. Publ. 248, p. 247-263.
- Henley R.W., Brink F.J., King P.L., Leys C., Ganguly J., Mernagh T., Middleton J., Renggli J.C., Sieber M., Troitzsch U., Turner M. (2017) High temperature gas-solid reactions in calc-silicate Cu-Au skarn formation; Ertsberg, Papua Province, Indonesia. *Contrib. Mineral. Petrol.*, 172:106. (<https://doi.org/10.1007/s00410-017-1413-6>)
- Hurai V., Huraiová M., Slobodník M., Thomas R. (2015) *Geofluids - Developments in Microthermometry, Spectroscopy, Thermodynamics, and Stable Isotopes*. Elsevier, 489p.
- Hollister V.F. (1975) An appraisal of the nature and source of porphyry copper deposits. *Min. Sci. Eng.*, 7, p. 225-233.
- Hovland M., Rueslåtten H., Johnsen H.K. (2014) Buried hydrothermal systems: the potential role of supercritical water," ScriW", in various geological processes and occurrences in the sub-surface. *Amer. Jour. of Analytical Chem.*, 5, p. 128-139.
- Ianovici V., Vlad Ș., Borcoș M., Boștinescu S. (1977) Alpine porphyry copper mineralization of West Romania. *Mineralium Deposita*, 12(3), p. 307-317. DOI:10.1007/bf00206169.
- Ilinca G., Berza T., Iancu V., Seghedi A. (2011) The late Cretaceous magmatic and metallogenetic belt and the alpine structures of the western south Carpathians. Field trip guide book. The 3rd Int. Symp. on the Geol. of the Black Sea Region, 1-10 oct. 2011, Bucharest, Romania.
- Ilinca G. (2012) Upper Cretaceous contact metamorphism and related mineralization in Romania. *Acta Mineralogica-Petrographica, Abstract Series, Szeged*, 7, p. 59-64.
- Knipping J.L., Bilenker L.D., Simon A.C., Reich M., Barro F., Deditius A.P., Wälle M. Heinrich C.A., Holtz F., Munizaga R. (2015) Trace elements in magnetite from massive iron oxide-apatite deposits indicate a combined formation by igneous and magmatic-hydrothermal processes. *Geochim. et Cosmochim. Acta*, 171, p. 15-38.
- Knipping J.L., Webster J.D., Simon A.C., Holtz F. (2019) Accumulation of magnetite by flotation on bubbles during decompression of silicate magmas. *Scientific Reports* 2019 March 7, 91, p. 3852.
- Koděra P., Heinrich C.A., Fallick A.E., Lexa J., Biroň A. (2014) Magmatic salt and vapor: Extreme fluids forming porphyry gold deposits in shallow subvolcanic settings. *Geology*, 42, 6, p. 495-498.
- Koděra P., Tacách Á., Racek M., Šimko F., Luptáková I., Váczi T., Antal P. (2017) Javorieite, KFeCl₃: a new mineral hosted by salt melt inclusions in porphyry gold systems. *Eur. J. Mineral.*, 6, p. 995-1004.
- Kontak D.J. (2004) Analysis of evaporate mounds as a complement to fluid-inclusion - thermometric data: case studies from granitic environments in Nova Scotia and Peru. *Canadian Mineralogist*, v. 42, p. 1315-1327.
- Kontak D.J. (2013) Fluid inclusion evaporate mound analysis: a rapid, efficient and informative means of determining fluid chemistry in hydrothermal systems. *Atlantic Geol.*, 49, 1, p. 34.
- Kotel'nikova Z.A., Kotel'nikov A.R. (2010) Experimental study of heterogeneous fluid equilibria in silicate-salt-water systems. *Geol. of Ore Dep.*, 52, 2, p. 154-166.
- Kotel'nikova Z.A., Kotel'nikov A.R. (2011) Na₂CO₃-bearing fluids: Experimental study at 700°C and under 1, 2, and 3kbar pressure using synthetic fluid inclusions in quartz. *Geol. of Ore Dep.*, 53, 2, p. 156-170.
- Kotel'nikova Z.A., Kotel'nikov A.R. (2016) Immiscibility in sulphide-bearing fluid systems at high temperatures and pressures. *Geochem. Internat.*, 48, 4, p. 381-389.
- Kouzmanov K., Pettke T., Heinrich C.A. (2010) Direct Analysis of Ore-Precipitating Fluids: Combined IR Microscopy and LA-ICP-MS Study of Fluid Inclusions in Opaque Ore Minerals. *Econ. Geol.*, 105, p. 351-373.
- Kouzmanov K., Pokrovsky G.S. (2012) Hydrothermal controls on metal distribution in porphyry Cu-Mo-Au systems. *Soc. Econ. Geol., Inc., Spec. Publ.*, 16, p. 573-618.
- Kozák J., Koděra P., Lexa J., Bakos F., Molnár L., Wälle M. (2017) Porphyry gold system of Beluj in the mantle of the Štiavnica stratovolcano Slovakia. *Acta Geol., Slovaca*, 9, 1, p. 45-61.
- Lerchbaumer L., Audétat A. (2012) High Cu concentrations in vapor-type fluid inclusions: an artifact? *Geochim. et Cosmochim. Acta*, 88, p. 255-274.
- Li Y., Audétat A., Lerchbaumer L., Xiong X.L. (2009) Rapid Na, Cu exchange between synthetic fluid inclusions and external aqueous solutions: evidence from LA-ICP-MS analysis. *Geofluids*, 9, p. 321-329.
- Lowell, J.D., Guilbert, J.M. (1970) Lateral and vertical alteration-mineralization zoning in porphyry ore deposits: *Econ. Geol.*, v. 65, p. 373-408.
- Lowenstern J.B. (1993) Evidence for a copper-bearing fluid in magma erupted at the Valley of Ten Thousand Smokes, Alaska. *Contrib. Mineral. Petrol.*, 114, 3, p. 409- 421.
- Mavrogenes J., Bodnar R.R. (1994) Hydrogen movement into and out of fluid inclusions in quartz: Experimental evidence and geologic implications. *Geochim. et Cosmochim. Acta*, 58(1), p. 141-148.
- Mernagh T.P., Mavrogenes J. (2019) Significance of high temperature fluids and melts in the Grasberg porphyry copper-gold deposit. *Chem. Geol.*, 508, p. 210-224.
- Momma K. (2014) Clathrate compound of silica. *J. Phys.: Condens. Matter* 26 20141032013, 18p.

- Mungall J.E., Brenan J.M., Godel B., Barnes S.J., Gaillard F. (2015) Transport of metals and sulphur in magmas by flotation of sulphide melt on vapour bubbles. *Nat. Geosci.*, 8, p. 216-219.
- Nash T.J. (1976) Fluid inclusion petrology-data from porphyry copper deposits and applications to exploration. U.S. Geol. Survey, Prof. Paper, 907-D, 16 p.
- Pintea I. (1993) Microthermometry of the hydrosaline melt inclusions from copper - porphyry ore deposits Apuseni Mountains, Romania. *Arch. Mineral.* XLIX, p. 165-167, Warsaw, Poland.
- Pintea I. (1995) Fluid inclusion evidence for magmatic immiscibility between hydrous salt melt and silicate melt as primary source of ore metals in porphyry copper system from Apuseni Mountains, Romania. *Bol. Soc. Espagnola Mineralogia*, 18 - 1, p. 184-186, Barcelona *and* Rom. Jour. of Mineralogy 77/2, suppl. pages.
- Pintea I. (1996a) New aspects of fluid phase evolution during genesis of the porphyry copper ore deposits from South Apuseni as seen in fluid inclusions. *Ann. IGR.*, 69, Suppl. 1, 166, Bucharest.
- Pintea I. (1996b) Fluid inclusion study with special view on immiscibility of the fluid phases associated in porphyry copper genesis from Apuseni Mountains. PhD thesis, Bucharest Univ., 172 p (in Romanian, unpublished).
- Pintea I. (1997) The significance of the liquid homogenisation temperature in salt melt inclusions. A case study in Neogene porphyry copper ore deposits from Metaliferi Mountains western Romania. *ECROFI-XIV*, Nancy, France July 1-4, Abstr. Vol., p. 266.
- Pintea I. (2002) Occurrence and microthermometry of the globular sulfide melt inclusions from extrusive and intrusive volcanic rocks and related ore deposits from Alpine Carpathian chain Romania "Volcanic Systems - Geochemistry and Geophysics Monitoring" Workshop - Napoli, Italy. Short Course, *Proced.*, Abstr. vol., p. 177-180.
- Pintea I. (2009) Still problematic facts on the fate of brines in the Alpine porphyry copper systems in Romania. *ECROFI XX*, Granada, Spain, Abstr. vol., p. 187 - 188.
- Pintea I. (2010) Fluid and melt inclusions evidences for autometasomatism and remelting in the Alpine porphyry copper genesis from Romania. The 7th Nat. Symp. on Econ. Geol., "Mineral Resources of Carpathian area", 10 - 12 Sept. 2010, Baia Mare. *Romanian Journal of Mineral Deposits*, Vol. 84, Spec. issue, p. 15-18.
- Pintea. I. (2012) Fluid and melt inclusions: a precious tool in selective exploration strategy. *Rom. J. of Mineral Dep.*, 85, 1, p. 85-89.
- Pintea I. (2014) The magmatic immiscibility between silicate-, brine-, and Fe-S-O melts from the porphyry Cu-(Au)-(Mo) deposits in the Carpathians Romania: a review. *Rom. J. of Earth Sci.* 87, 1, online first, 32p.
- Pintea I. (2016) A self-perspective research topic revealed during the elaboration of the Atlas "Fluid and Melt Inclusions from Romania". *Rom. J. of Min. Dep.*, 89, 1-2, p. 1-6.
- Pintea I., Laczko A.A. (2005) Preliminary microthermometric data related to a complex magmatic-hydrothermal system from Sântimbru-Băi South-Harghita Mountains, Romania. *Geol. Soc. Romania meeting, Rosia Montana, Romania, Proceed.* Vol., p. 25-96.
- Pintea I., Nuțu-Dragomir M.-L., Udubașa S.S., Bîrgăoanu D., Iatan E.L., Berbelec I., Ciobotea-Barbu O.C. (2018) Hydrosilicate aqueous-, and vapor- "melt" inclusions in some specific rocks and minerals from Romania. *Rom. J. of Min. Dep.*, 91, 1-2, p. 13-18.
- Pintea I., Udubașa G., Nedelcu L. (1999) Evolution of fluid phases related to a new porphyry copper deposit in Romania: The Tibles massif. In: Stanley et al. (eds) *Mineral Deposits: Processes to Processing*, Balkema, Rotterdam, p. 83-85.
- Pintea I., Udubasa S.S., Nutu-Dragomir L. M., Iatan E.L., Berbelec I., Petrescu L., Ghinescu E. (2019) Clathrasil compound evidence in fluid and brine inclusions by microthermometry and Raman spectroscopy. *Goldschmidt Conference 2019, Barcelona, Spain*, abstract online.
- Pirajno F. (2009) *Hydrothermal processes and mineral systems*. Springer Science+Media B.V., 1273p.
- Pomârleanu V., Intorsureanu I. (1985) Salinity of fluid inclusions of porphyry copper ore deposits and their significance in geobarometry and prospecting the Lăpușnicu Mare ore deposit - Banat. *D.S. Inst. Geol. Geofiz.*, 70-71/2 (1983; 1984), p. 83-95.
- Ramboz C. (1979) A fluid inclusion study of the copper mineralization in Southwest Tintic district Utah. *Bull. Mineral.*, 102, p. 622-632.
- Redmond P.B., Einaudi M.T., Inan E.E., Landtwing M.R., Heinrich C.A. (2004) Copper deposition by fluid cooling in intrusion-centered systems: New insights from the Bingham porphyry ore deposit, Utah. *Geology*, 32, 3, p. 217-220.
- Renno A.D., Franz L., Witzke T., Herzig P.M. (2004) The coexistence of melts of hydrous copper chloride, sulphide and silicate compositions in a magnesiohastingsite cumulate, TUBA Seamount, Papua New Guinea. *The Canadian Mineralogist.*, 42, p. 1-16.
- Richards J.P. (2009) Postsubduction porphyry Cu-Au and epithermal Au deposits: Products of remelting of subduction-modified lithosphere. *Geology*, 37, p. 247-250.
- Roedder E. (1971) Fluid inclusion studies on the porphyry type ore deposits at Bingham Utah, Butte Montana and Climax Colorado. *Econ. Geol.*, 66, p. 98-120.
- Roedder E. (1984) Fluid inclusions. *Reviews in Mineralogy*, 12, 644 p.
- Roedder E., Bodnar R.J. (1980) Geologic pressure determinations from fluid inclusion studies. *Earth Planet. Sci., Ann. Rev.*, 8, p. 263-301.

- Roşu E., Seghedi I., Downes H., Alderton D.H.M., Szakács A., Péckaj Z., Panaiotu C., Panaiotu E.C., Nedelcu L. (2004) Extension-related Miocene calc-alkaline magmatism in the Apuseni Mountains, Romania: origin of magmas. *Schw. Miner. Petrogr. Mitt.* 84, p. 153-172.
- Sanchez-Lecumberri P., Steele-McInnis M., Bodnar R.J. (2012) A numerical model to estimate trapping conditions of fluid inclusions that homogenize by halite disappearance. *Geochim. et Cosmochim. Acta*, 92, p. 14-22.
- Seo J.H., Heinrich C.A. (2013) Selective copper diffusion into quartz-hosted vapour inclusions: evidence from other host minerals, driving forces and consequences for Cu-Au ore formation. *Geochim. et Cosmochim. Acta*, 113, p. 60-69.
- Sillitoe R.H. (2010) Porphyry copper systems. *Economic Geology*, v. 105, p. 3–41.
- Smirnov S.Z., Thomas V.G., Kamenetsky V.S., Kozmenko O.A. (2017) Hydrosilicate liquids in the system rare-metal granite-Na₂O-SiO₂-H₂O as accumulators of ore components at high pressure and temperature. *Petrology*, 25, 6, p. 625-635.
- Spencer E.T., Wilkinson J.J., Nolan J., Berry A.J. (2015) The control of post-entrapment diffusion on the solubility of chalcopyrite daughter crystals in natural quartz-hosted fluid inclusions. *Chem. Geol.*, 412, p. 15-25.
- Steele-MacInnis M., Sanchez-Lecumberri P., Bodnar J.R. (2012) HokieFlincs-H₂O-NaCl: a microsoft Excel spreadsheet for interpreting microthermometric data from fluid inclusions based on the PVTX properties of H₂O-NaCl. *Computers and Geosci.*, 49, p. 334-337.
- Stefanova E., Driesner T., Zajaz Z., Heinrich C.A., Petrov P., Vasiliev Z. (2014) Melt and fluid inclusions in hydrothermal veins: the magmatic to hydrothermal evolution of the Elatsite porphyry Cu-Au deposit, Bulgaria. *Econ. Geol.*, 109, p. 1359-1381.
- Sterner M.S., Bodnar R.J. (1987) Synthetic fluid inclusions. In *Hydrothermal experimental techniques* (Ulmer G.C., Barnes H.L., eds), p. p. 423-457.
- Thomas R., Davidson P. (2016) Revisiting complete miscibility between silicate melts and hydrous fluids, and the extreme enrichment of some elements in the supercritical state - Consequences for the formation of pegmatite and ore deposits. *Ore Geol. Rev.*, 72, p. 1088-1101.
- Tornos F., Velasco F., Hanchar J.M. (2016) Iron-rich melts, magmatic magnetite, and superheated hydrothermal systems: The El Laco deposit, Chile. *Geology*, 44, 6, p. 427-430.
- Tweedale F., Hanley J.J., Kontak D.J., Rogers N. (2015) Petrographic observations and evaporate mound analysis of quartz-hosted fluid inclusions hosted by granitoid samples from the South Mountain Batholith, Nova Scotia: An exploration tool for vectoring towards mineralised areas in intrusive rocks. In: Rogers N. (ed.) *TGI4 – Intrusion Related Mineralisation Project: New Vectors to Buried Porphyry-Style Mineralisation*. Geological Survey of Canada, Open File 7843, p. 79-99.
- Udubaşa G., Roşu E., Seghedi I., Ivăşcanu P.M. (2001) The “Golden Quadrangle” in the Metaliferi Mts., Romania: what does this really mean? *ABCD-GEODE Workshop, Vaţa Băi, Romania*. *Rom. J. Miner. Dep.*, 79, suppl 2, p. 24-34.
- Vlad S.N. (2011) Perspective targeting CuAuMo porphyries of Romanian Carpathians: blind porphyry mineralization and its variable distal expression as vein and skarns. *Cent. Eur. J. Geosci.*, 3(3), p. 318-335.
- Vlad Ş-N, Berza T. (2003) Banatitic magmatic and metallogenetic belt: metallogeny of the Romanian Carpathians segment. *Studia Universitatis Babeş-Bolyai, Geologia*, XLVIII, 1, 2003, p. 113-122.
- Weisbrod A. (1981) Fluid inclusions in shallow intrusives. In: Hollister L.S., Crawford M.L. (eds) *Mineral. Assoc. of Canada, Short course handbook 6*, p. 241-271.
- Wilkinson J.J., Nolan J., Rankin A.H. (1996) Silicothermal fluid: a novel medium for mass transport in the lithosphere. *Geology*, 24, p. 1059-1062.
- Wilkinson J.J., Vasyukova O., Laird J.S., Ryan C., Kamenetsky D. (2015) Hydrosilicate liquids: unconventional agents of metal transport in porphyry ore systems. *ECROFI, Leeds-UK, 27-29 June, 2015, Extended Abstracts Volume*, p. 116.
- Zimmerman A., Stein H.J., Hannah J.L., Koželi D., Bogdanov K., Berza T. (2008) Tectonic configuration of the Apuseni-Banat-Timok–Srednogorie belt, Balkans-South Carpathians, constrained by high precision Re–Os molybdenite ages. *Miner Deposita*, 43, p. 1-21.